Inverse problems in functional brain imaging.

Reference material for the MVA Master 2 class

Maureen Clerc
Théo Papadopoulo
(section on fMRI analysis adapted from Bertrand Thirion's PhD thesis)

December 12, 2008

Contents

Chapter 1

Introduction

The study of human bioelectricity was initiated with the discovery of electrocardiography at the turn of the twentieth century, followed by electroencephalography (EEG) in the 1920's, magnetocardiography in the 1960's, and magnetoencephalography (MEG) in the 1970's. Biomagnetic and bioelectric fields have the same biological origin: the displacement of charges within active cells called neurons [13].

Nowadays, EEG is relatively inexpensive and used commonly to detect and qualify neural activities (epilepsy detection and characterisation, neural disorder qualification, Brain Computer Interfaces, ...). MEG is, comparatively, much more expensive as SQUIDS work in very challenging conditions (at liquid helium temperature) and as a specially shielded room must be used to separate the signal of interest from the ambient noise. However, as it reveals a complementary vision to that of EEG and as it is less sensitive to the head structure, it also bears great hopes and more and more MEG machines are installed throughout the world.

There are several scales at which bioelectricity can be described and measured: the microscopic scale, with microelectrodes placed inside or in a very close vicinity to neurons, and the mesoscopic scale, with intracortical recording of local field potentials (i.e. the electric potential within the cortex), below a square millimeter. Non-invasive measurements of the electric potential via EEG or the magnetic field via MEG are taken on the scalp, and the spatial extent of brain activity to which these measurements can be related has not yet been elucidated, but lies between a square millimeter and a square centimeter. Given the size of the head, and the time scale of interest - the millisecond - the quasistatic approximation can be applied to the Maxwell equations [10]. The electromagnetic field is thus related to the electric sources by two linear equations: the Poisson equation for the electric potential, and the Biot-Savart equation for the magnetic field.

MEG and EEG can be measured simultaneously and reveal complementary properties of the electrical fields. The two techniques have temporal resolutions of about the millisecond, which is the typical granularity of the measurable electrical phenomenons that arise in the brain. This high temporal resolution is what makes MEG and EEG attractive for the functional study of the brain. The spatial resolution, on the contrary, is somewhat poor as only a few hundreds of simultaneous data points can be acquired simultaneously (about 300-400 for MEG and up to 256 for EEG). MEG and EEG are somewhat complementary with fMRI and

SPECT in that those provide a very good spatial resolution but a rather poor temporal one (about the second for fMRI and the minute for SPECT). Contrarily to fMRI, which "only" measures an haemodynamic response linked to the metabolic demand, MEG and EEG also measure a direct consequence of the electrical activity of the brain: it is admitted that the MEG and EEG measured signals correspond to the variations of the post-synaptic potentials of the pyramidal cells in the cortex. Pyramidal neurons compose approximately 80% of the neurons of the cortex, and it requires at least about 50,000 active such neurons to generate some measurable signal.

Reconstructing the cortical sources from the electromagnetic field measured on EEG and MEG sensors requires that the inverse problem of MEG and EEG (denoted collectively as MEEG for short) be solved. It is a difficult problem because it is ill-posed, and this has led to a large body of literature, concerning both theoretical [3, 5] and computational aspects [2, 6, 8].

There are two main domains of application for EEG and MEG: clinical applications and the study of cognition.

Clinical research in neurophysiology aims at understanding the mechanisms leading to disorders of the brain and the central nervous system, in order to improve diagnosis and eventually propose new therapies. The clinical domains in which EEG and MEG are most routinely used include epilepsy, schizophrenia, depression, attention deficit disorders. Clinicians are especially interested in the time courses of the measured signals: their experience in the visual analysis of superimposed sensor time courses allows them to detect abnormal patterns. The source localization performed by clinicians is generally limited to simple dipole scanning methods.

EEG and MEG rely on passive measurements, with no applied electromagnetic field. In contrast, active techniques using bioelectric stimulation, are currently being developed and tested on patients, to treat disorders such as Parkinson's disease, chronic pain, dystonia and depression. Implanted intracortical or extradural electrodes can deliver a electrical stimulation to specific brain areas (Deep Brain Stimulation or DBS). Less invasive, Transcranial Magnetic Stimulation (TMS), uses a time-varying magnetic field to induce a current within the cortex. All of these techniques can be studied with the same equations, models, and numerical tools as the ones used for MEEG. Moreover, in order to understand the physiological mechanisms triggered by these stimulations, simultaneous TMS/EEG and DBS/MEEG can be performed and analyzed [16].

In cognitive neuroscience, much of our knowledge of the brain has been acquired from intracortical recordings in cat and monkey brains, as well as peroperative recordings on human brains. Although the advent of functional Magnetic Resonance Imaging (fMRI) in the 1980's has opened a unique perspective on the localization of human brain cognitive function, timing issues remain difficult to resolve. Because of their high time resolution, EEG and MEG are very useful for analyzing oscillatory activity, and the timings of activations between different brain regions. And because of its strictly non-invasive nature, MEEG is also well-suited to the study of the development of human brain function, from infancy to adulthood.

This class material is divided in two parts: the first on models for MEG and EEG, which goes into details in explaining geometrical, physiological and numerical models used in this field. The second part deals with the analysis of functional imaging data, coming from fMRI or from MEG/EEG.

Part I

Magneto-electroencephalography models

Chapter 2

Electromagnetic propagation

Neuronal currents generate magnetic and electric fields according to principles stated in Maxwell's equations. The neural current distribution can be described as the primary current, and viewed as the "battery" in a resistive circuit. The postsynaptic currents in the cortical pyramidal cells are the main primary currents which give rise to measurable MEEG signals.

2.1 Maxwell equations

2.1.1 Current density

The current density $\mathbf{J}$ represents the current crossing a unit surface normal to $\mathbf{J}$. Its unit is $A \cdot m^{-2}$. The total intensity crossing an oriented surface S is

$$I = \int_S \mathbf{J} \cdot \mathbf{n} \, ds \ .$$

The electric charge conservation principle attributes the variation of charge inside a closed surface exclusively to exchanges with the outside medium. Let ρ denote the volumic charge density. For a closed surface, the orientation convention is for the normal vector to point outward. The charge conservation principle implies that, if Ω is a volume with boundary $\partial\Omega$,

$$\frac{d}{dt} \int_\Omega \rho \, d\mathbf{r} = - \int_{\partial\Omega} \mathbf{J} \cdot \mathbf{n} \, ds \tag{2.1}$$

For a fixed volume Ω,

$$\frac{d}{dt} \int_\Omega \rho \, d\mathbf{r} = \int_\Omega \frac{\partial \rho}{\partial t} \, d\mathbf{r} \tag{2.2}$$

The Green identity implies that

$$\int_{\partial\Omega} \mathbf{J} \cdot \mathbf{n} \, ds = \int_\Omega \nabla \cdot \mathbf{J} \, d\mathbf{r} \tag{2.3}$$

and replacing (2.2) and (2.3) in (2.1),

$$\int_\Omega \frac{\partial \rho}{\partial t}\, d\mathbf{r} = -\int_\Omega \nabla \cdot \mathbf{J}\, d\mathbf{r}$$

As this is true for any fixed volume Ω, we obtain the local charge conservation equation:

$$\nabla \cdot \mathbf{J} = -\frac{\partial \rho}{\partial t} \tag{2.4}$$

2.1.2 Maxwell-Gauss equation

The electric field generated at a position M by a single charge q_i at position P_i is equal to

$$\frac{1}{4\pi\varepsilon_0} q_i \frac{\overrightarrow{P_iM}}{\|P_iM\|^3}$$

where ε_0 is the electrical permitivity of the vacuum. The flow of the electric field across a surface S is defined by $\psi = \int_S \mathbf{E} \cdot \mathbf{n}\, ds$. The electric flow on S due to a charge q positioned at P (coordinate $\mathbf{p}$) is hence equal to

$$\psi = \frac{q}{4\pi\varepsilon_0} \int_S \frac{\mathbf{r}-\mathbf{p}}{\|\mathbf{r}-\mathbf{p}\|^3} \cdot \mathbf{n}\, ds = \frac{q}{4\pi\varepsilon_0}\Omega$$

where Ω is the solid angle spanning S from position P.

For a closed surface S, $\Omega = 0$ if P is outside S, and $\Omega = 4\pi$ if P is inside S. The electric flow generated on a surface S by a set of charges q_i is, by summation, equal to

$$\psi = \frac{1}{4\pi\varepsilon_0} \sum q_i\, \Omega_i$$

where Ω_i is equal to 0 (resp. 4π) if the corresponding charge is outside (resp. inside) S. This result leads to the Gauss theorem:

$$\int_{\partial\Omega} \mathbf{E} \cdot \mathbf{n}\, ds = \frac{Q_{int}}{\varepsilon_0} = \int_\Omega \frac{\rho}{\varepsilon_0}\, d\mathbf{r}$$

where ρ is the (volumic) charge density. Using the Green identity, the above relation becomes

$$\int_\Omega \nabla \cdot \mathbf{E}\, d\mathbf{r} = \int_\Omega \frac{\rho}{\varepsilon_0}\, d\mathbf{r}\ ,$$

which provides, in its local version, the Maxwell-Gauss equation:

$$\nabla \cdot \mathbf{E} = \frac{\rho}{\varepsilon_0}\ . \tag{2.5}$$

2.1.3 Maxwell-Ampere equation

Ampere's law is first established for a time-invariant setting. Given a closed loop enclosing an open surface S, the magnetic field integrated along ∂S is proportional to the current I crossing S:

$$\int_{\partial S} \mathbf{B} \cdot \overrightarrow{dl} = \mu_0 I\ .$$

The coefficient μ_0 is the magnetic susceptibility of the vacuum (ε_0 and μ_0 statisfy the relation $\varepsilon_0\mu_0c^2 = 1$). Using Green's (Stokes) theorem and introducing the current density $\mathbf{J}$, the above relation becomes

$$\int_S \nabla \times \mathbf{B} \cdot \mathbf{n}\, ds = \mu_0 \int_S \mathbf{J} \cdot \mathbf{n}\, ds$$

As this must hold for any open surface S, this implies the local relationship:

$$\nabla \times \mathbf{B} = \mu_0 \mathbf{J} \ . \tag{2.6}$$

As a consequence, the current density must be divergence-free:

$$\nabla \cdot \mathbf{J} = 0 \ .$$

We have seen in 2.1.1 that the charge conservation principle implies

$$\nabla \cdot \mathbf{J} = -\frac{\partial \rho}{\partial t} \ .$$

Using the Maxwell-Gauss equation (2.5),

$$\nabla \cdot \mathbf{J} = -\nabla \cdot \varepsilon_0 \frac{\partial \mathbf{E}}{\partial t}$$

In the time-variant case, the quantity which is divergence-free is no longer the current density, but

$$\mathbf{J} + \varepsilon_0 \frac{\partial \mathbf{E}}{\partial t} \ .$$

Ampere's law (2.6) must be adapted to account for the additional term $\varepsilon_0 \frac{\partial \mathbf{E}}{\partial t}$, sometimes called "displacement current". This leads to the Maxwell-Ampere equation:

$$\nabla \times \mathbf{B} = \mu_0 \left(\mathbf{J} + \varepsilon_0 \frac{\partial \mathbf{E}}{\partial t} \right) \tag{2.7}$$

2.1.4 Maxwell-Faraday equation

The Maxwell-Faraday equation is a structural relationship between the electric and magnetic fields. Consider the electric force

$$e(t) = \int_{\partial S} \mathbf{E} \cdot \overrightarrow{dl}$$

induced by a magnetic field $\mathbf{B}$ on a lineic circuit enclosing an open surface S. The law of induction states that

$$e(t) = -\frac{d\phi}{dt}$$

where

$$\phi(t) = \int_S \mathbf{B} \cdot \mathbf{n}\, ds.$$

The Green (Stokes) theorem provides the local form of the induction theorem, called the Maxwell-Faraday equation:

$$\nabla \times \mathbf{E} = -\frac{\partial \mathbf{B}}{\partial t} \tag{2.8}$$

2.1.5 Maxwell-Gauss equation for magnetism

The last Maxwell equation is a conservation equation for the magnetic field, which basically states the absence of magnetic monopoles. In its local form, it is writeen as:

$$\nabla \cdot \mathbf{B} = 0 \, . \tag{2.9}$$

The integral form of this equation being:

$$\int_{\partial\Omega} \mathbf{B} \cdot \mathbf{n} \, ds = 0 \, .$$

2.1.6 Summary

The local and integral forms of the Maxwell equations are summarized in table:

Name	Differential form	Integral form
Gauss's law	$\nabla \cdot \mathbf{E} = \frac{\rho}{\varepsilon_0}$	$\int_{\partial\Omega} \mathbf{E} \cdot \mathbf{n} \, ds = \int_{\Omega} \frac{\rho}{\varepsilon_0} \, d\mathbf{r}$
Gauss's law for magnetism	$\nabla \cdot \mathbf{B} = 0$	$\int_{\partial\Omega} \mathbf{B} \cdot \mathbf{n} \, ds = 0$
Faraday's law	$\nabla \times \mathbf{E} = -\frac{\partial \mathbf{B}}{\partial t}$	$\int_{\partial S} \mathbf{E} \cdot \overrightarrow{dl} = -\int_S \frac{\partial \mathbf{B}}{\partial t} ds$
Ampère's circuital law	$\nabla \times \mathbf{B} = \mu_0 \left(\mathbf{J} + \varepsilon_0 \frac{\partial \mathbf{E}}{\partial t} \right)$	$\int_{\partial S} \mathbf{B} \cdot \overrightarrow{dl} = \mu_0 \int_S \left(\mathbf{J} + \varepsilon_0 \frac{\partial \mathbf{E}}{\partial t} \right) \cdot \mathbf{n} \, ds$

2.2 Quasistatic approximation

The Maxwell equations were presented above in a general, time-varying, setting. For EEG and MEG modeling, the spatial scale, the frequencies, and the medium properties make it possible to neglect the inductive, capacitive and displacement effects, and to effectively omit the time-derivatives in (2.7) and (2.8). Omitting the time-derivatives in (2.7) is called quasi-stationariry while omitting the time-derivatives in both (2.7) and (2.8) is called the quasistatic regime. This considerably simplifies the resulting system, because the magnetic and electric fields become uncoupled, and can be solved separately.

Let us briefly justify the quasistatic assumption. We note that, in a magnetic medium free of charges or current generators, the volumic current density $\mathbf{J}$ is the sum of an *volumic ohmic current* and a *polarization current*:

$$\mathbf{J} = \sigma \mathbf{E} + \frac{\partial \mathbf{P}}{\partial t} \tag{2.10}$$

where $\mathbf{P} = (\epsilon - \epsilon_0) \, \mathbf{E}$ is the polarization vector, ϵ the *permittivity* of the medium, and σ the *conductivity*.

Let us examine the Maxwell-Ampere equation (2.7). Using (2.10), we are able to express the right-hand side as a function of $\mathbf{E}$ only:

$$\nabla \times \mathbf{B} = \mu_0 \left(\sigma \, \mathbf{E} + \varepsilon \frac{\partial \mathbf{E}}{\partial t} \right)$$

Let us further assume that the electrical field can be modelled using a planar waveform at frequency f, $\mathbf{E}(\mathbf{r},t) = \mathbf{E}_0 e^{i(\omega t - \mathbf{k}\cdot\mathbf{r})}$, with $\omega = 2\pi f$ and the added condition $\mathbf{E}_0 \cdot \mathbf{k} = 0$.

Using this model, we have:

$$\frac{\partial \mathbf{E}}{\partial t} = i\omega \mathbf{E}$$

and

$$\begin{aligned} \left\| \varepsilon \frac{\partial \mathbf{E}}{\partial t} \right\| &= \omega\varepsilon \|\mathbf{E}\| \\ \|\sigma \mathbf{E}\| &= \sigma \|\mathbf{E}\| \end{aligned}$$

The term $\varepsilon \frac{\partial \mathbf{E}}{\partial t}$ is negligible compared to $\sigma\,\mathbf{E}$, at a frequency f, if

$$\frac{2\pi\, f\, \varepsilon}{\sigma} \ll 1 \ .$$

For the brain, $\sigma = 0.3\,\Omega^{-1}m^{-1}$, the permittivity ε is of the order of $10^5\varepsilon_0 = 8.8510^{-7}$, and the frequencies of interest are typically lower than $f = 100$ Hz. With these values, $\frac{2\pi\, f\, \varepsilon}{\sigma}$ is of the order of $2 \cdot 10^{-3}$. Therefore, the time derivative in (2.7) can be neglected. The Maxwell-Ampere equation becomes time-invariant:

$$\nabla \times \mathbf{B} = \mu_0 \mathbf{J} \ , \tag{2.11}$$

and the current density is consequently divergence-free

$$\nabla \cdot \mathbf{J} = 0 \ . \tag{2.12}$$

To show that the time-derivative can be neglected in (2.8), we compute the rotational of this equation. The left hand side becomes:

$$\nabla \times (\nabla \times \mathbf{E}) = \nabla(\nabla \cdot \mathbf{E}) - \Delta \mathbf{E} \ .$$

But with our choice for $\mathbf{E}$, we have:

$$\nabla \cdot \mathbf{E} = \mathbf{E}_0 \nabla e^{i(\omega t - \mathbf{k}\cdot\mathbf{r})} = -i\mathbf{E}_0 \cdot \mathbf{k} e^{i(\omega t - \mathbf{k}\cdot\mathbf{r})} = 0 \ .$$

Thus:

$$\begin{aligned} \nabla \times (\nabla \times \mathbf{E}) = -\Delta \mathbf{E} = -\|\mathbf{k}\|^2 \mathbf{E} &= -\frac{\partial}{\partial t} \nabla \times \mathbf{B} \\ &= -\mu_0 \frac{\partial}{\partial t} \left(\sigma \mathbf{E} + \varepsilon \frac{\partial \mathbf{E}}{\partial t} \right) \\ &= -\mu_0 i\omega(\sigma + \varepsilon i\omega)\mathbf{E} \end{aligned}$$

Consequently, we get: $\|\mathbf{k}\|^2 = |\mu_0 i\omega(\sigma + \varepsilon i\omega)|$ and the corresponding wavelength is $\lambda = \frac{1}{\|\mathbf{k}\|} = \frac{1}{\sqrt{|\mu_0 i\omega(\sigma+\varepsilon i\omega)|}}$. For the head, this quantity is equal to $65m \gg \varnothing$head. This means that the time-derivative can be neglected in (2.8), leading to the time-invariant Maxwell-Faraday equation

$$\nabla \times \mathbf{E} = 0 \ . \tag{2.13}$$

2.2.1 Poisson equation

A consequence of the time-invariant Maxwell-Faraday equation (2.13) is that the electric field $\mathbf{E}$ derives from a potential, which we call the electric potential and denote V:

$$\mathbf{E} = -\nabla V \ .$$

It is useful to divide the current density $\mathbf{J}$, into two components: the passive *ohmic* or *return* current $\sigma\mathbf{E}$ and the remaining *primary current* $\mathbf{J}^{\mathrm{p}}$

$$\mathbf{J} = -\sigma\nabla V + \mathbf{J}^{\mathrm{p}}. \tag{2.14}$$

Although this equation holds at different scales, it is not possible to include all the microscopic conductivity details in models of MEEG activity and thus σ refers to macroscopic conductivity with at least $1mm$ scale. The division of neuronal currents to primary and volume currents is physiologically meaningful. For instance, chemical transmitters in a synapse give rise to primary current mainly inside the postsynaptic cell, whereas the volume current flows passively in the medium, with a distribution depending on the conductivity profile. By finding the primary current, we can locate the active brain regions.

The current density is divergence-free, and using the decomposition (2.14) shows that the electric potential and the primary current are related by a simple equation, called a Poisson equation:

$$\nabla \cdot (\sigma\nabla V) = \nabla \cdot \mathbf{J}^{\mathrm{p}} \ . \tag{2.15}$$

2.2.2 Biot and Savart law

We derive in this section the Biot and Savart law, relating the magnetic field to the current density. Recall the time-invariant Maxwell-Ampere equation

$$\nabla \times \mathbf{B} = \mu_0 \, \mathbf{J}$$

and take its curl:

$$\nabla \times \nabla \times \mathbf{B} = \mu_0 \, \nabla \times \mathbf{J} \ . \tag{2.16}$$

The left-hand side can be rewritten

$$\nabla \times \nabla \times \mathbf{B} = -\Delta\mathbf{B} + \nabla(\nabla \cdot \mathbf{B})$$

where the Laplacian acts coordinatewise on the vector field $\mathbf{B}$. Since $\nabla \cdot \mathbf{B} = 0$ (Maxwell equation expressing absence of magnetic charges), (2.16) rewrites:

$$-\Delta\mathbf{B} = \mu_0 \nabla \times \mathbf{J} \ .$$

Recalling that a fundamental solution fo the Laplacian in $\mathbb{R}^3$ is $-\frac{1}{4\pi\|r\|}$ (see appendix A.1.2), in the sense that

$$\Delta\left(-\frac{1}{4\pi\|r\|}\right) = \delta_0$$

this implies that

$$\mathbf{B} = \frac{\mu_0}{4\pi} \int \nabla \times \mathbf{J}(\mathbf{r}') \frac{1}{\|\mathbf{r} - \mathbf{r}'\|} \, d\mathbf{r}' + \mathbf{B}_H$$

where $\mathbf{B}_H$ is a *harmonic* function, i.e. such that

$$\Delta \mathbf{B}_H = 0 \ .$$

With the condition that $\mathbf{B}$ vanishes at infinity, the harmonic term can be discarded, an integration by parts leads to the Biot and Savart law:

$$\mathbf{B} = \frac{\mu_0}{4\pi} \int \mathbf{J}(\mathbf{r}') \times \frac{\mathbf{r} - \mathbf{r}'}{\|\mathbf{r} - \mathbf{r}'\|^3} \, d\mathbf{r}' \ . \tag{2.17}$$

Replacing the total current $\mathbf{J}$ by its decomposition (2.14), the Biot-Savart law becomes

$$\mathbf{B} = \mathbf{B}_0 - \frac{\mu_0}{4\pi} \int \sigma \nabla V \times \frac{\mathbf{r} - \mathbf{r}'}{\|\mathbf{r} - \mathbf{r}'\|^3} \, d\mathbf{r}' \ , \tag{2.18}$$

where $\mathbf{B}_0$ is the contribution to the magnetic field coming from the primary current:

$$\mathbf{B}_0 = \frac{\mu_0}{4\pi} \int \mathbf{J}^{\mathrm{p}} \times \frac{\mathbf{r} - \mathbf{r}'}{\|\mathbf{r} - \mathbf{r}'\|^3} \, d\mathbf{r}' \ .$$

Note: if the medium is infinite, with homogeneous conductivity σ, a simplification occurs in the Biot-Savart equation, since

$$\nabla \times \mathbf{J}(\mathbf{r}') = \nabla \times (\mathbf{J}^{\mathrm{p}} - \sigma \nabla V),$$

and in a homogeneous medium, $\nabla \times (\sigma \nabla V) = \sigma \nabla \times \nabla V = 0$. The magnetic field hence becomes independent of the ohmic contribution:

$$\mathbf{B} = \mathbf{B}_0 = \frac{\mu_0}{4\pi} \int \mathbf{J}^{\mathrm{p}} \times \frac{\mathbf{r} - \mathbf{r}'}{\|\mathbf{r} - \mathbf{r}'\|^3} \, d\mathbf{r}' \ . \tag{2.19}$$

2.3 Neural current sources

2.3.1 Action potentials and postsynaptic potentials

Electric signals propagate within the brain along nerve fibers (axons) as a series of action potentials (APs). The corresponding primary current can be approximated by a pair of opposite current dipoles, one at the depolarization and one at the repolarization front (figure), and this quadrupolar source moves along the axon as the activation propagates. The separation of the two dipoles depends on the duration of the AP and on the conduction velocity of the fiber. For a cortical axon with a conduction speed of 5 m/s, the opposite dipoles would be about 5mm apart.

In synapses, the chemical transmitter molecules change the ion permeabilities of the postsynaptic membrane and a postsynaptic potential (PSP) and current are generated. In contrast to the currents associated with an action potential, the postsynaptic current can be adequately described by a single current dipole oriented along the dendrite. The magnetic field of a current dipole falls off with distance

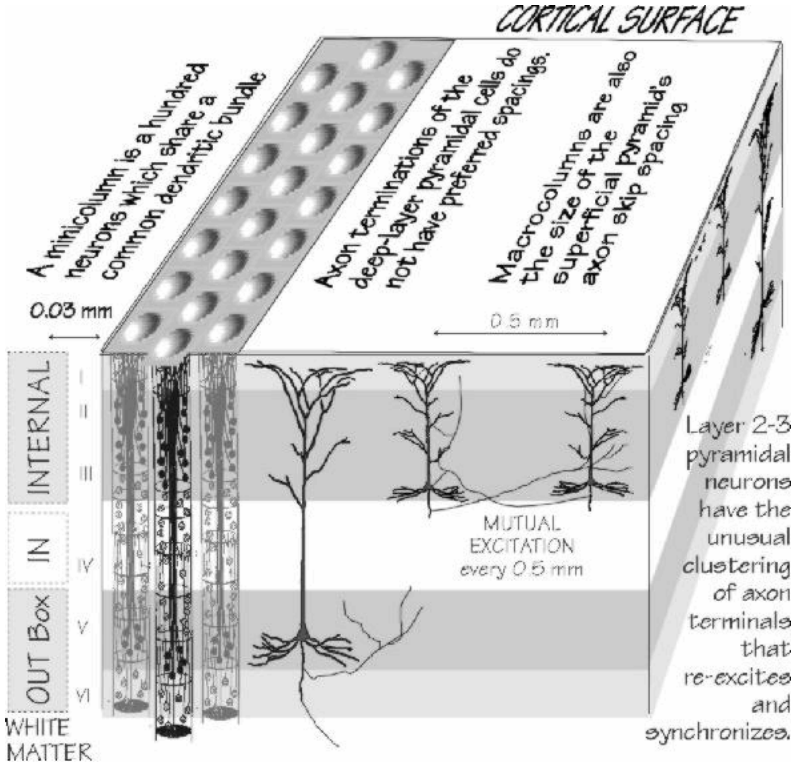

Figure 2.1: The organisation of the cortex.

more slowly (in order $1/r^2$) than the field associated with the quadrupolar AP currents (in order $1/r^3$).

Furthermore, temporal summation of currents flowing in neighboring fibers is more effective for synaptic currents, which last up to tens of milliseconds, than for the about 1 ms-long action potentials. Thus the electromagnetic signals observed outside and on the surface of the head seem to be largely due to the synaptic current flow. In special cases, currents related to action potentials might also significantly contribute to cortical MEG and EEG signals, such as, e.g., high-frequency somatosensory responses.

The pyramidal cells are the principal types of neurons in the cortex, with their apical dendrites oriented parallel to each other and perpendicular to the cortical surface. Since neurons guide the current flow, the resultant direction of the electrical current flowing in the dendrites is also perpendicular to the cortical sheet of gray matter.

2.3.2 Estimates of dipole strengths

Each PSP may contribute as little as a 20 fAm current dipole, probably too small to measure in MEEG. The current dipole moments required to explain the measured MEEG fields outside the head are on the order of 10 nAm[**?**]. This would correspond to about a million of synapses simultaneously active during a typical evoked

response. Although such a synchronous activity only forms a part of the total activity, it can be functionally highly important. For example, invasive recordings from monkeys have shown suprisingly large temporal overlap of neuronal firing in many visual cortical areas (Schmolesky et al, 1998). Epileptic discharges also are typically associated with strong current densities due to highly synchronous activity.

Chapter 3

Geometric modeling of the head

3.1 Magnetic Resonance Imaging

Magnetic resonance imaging (MRI) was developed from knowledge gained in the study of nuclear magnetic resonance. The acronym NMR (Nuclear Magnetic Resonance) is still often used to describe the technique.

3.1.1 Basic principle of NMR

MRI relies (most often) on the relaxation properties of excited hydrogen nuclei in water. Since hydrogen nuclei have a single proton, they have a spin, which is an intrinsic angular moment. It can be associated with a magnetic dipole moment: each hydrogen nucleus behaves as a tiny magnet, with the north/south axis parallel to the spin axis. The sum of the moments of a sample of molecules is zero in the absence of a magnetic field. When an object to be imaged is placed in the powerful, uniform magnetic field $\mathbf{B}_0$, the spins of the nuclei within the tissue precess around the direction of $\mathbf{B}_0$. The resulting magnetic moment of a sample is oriented in the direction of $\mathbf{B}_0$. The frequency ν_0 (Larmor frequency) of the precession is linearly related to the field by the gyromagnetic ratio γ, whose value depends on the nature of the nuclei.

$$\nu_0 = \gamma|\mathbf{B}_0| \tag{3.1}$$

Besides the precession of the nuclei, a second phenomenon is important to us: the relaxation of the nuclei. In the presence of a constant field $\mathbf{B}_0$, the spin axes of the nuclei slowly tend to align with $\mathbf{B}_0$. The Radio Frequency pulse (RF pulse) technique consists in applying in addition to $\mathbf{B}_0$ a transient field pulse $\mathbf{B}_1$, orthogonal to $\mathbf{B}_0$, rotating at the resonance frequency of the nuclei ν_0, and several orders of magnitude smaller. When such an RF pulse is applied the resulting moments M of the nuclei are flipped (usually by 30 or 90 degrees, according to the duration of the pulse). After the pulse, M precesses around $\mathbf{B}_0$ and finally aligns with $\mathbf{B}_0$: the transient transversal moment iM_T also called *Free Induction Decay* (FID) cancels

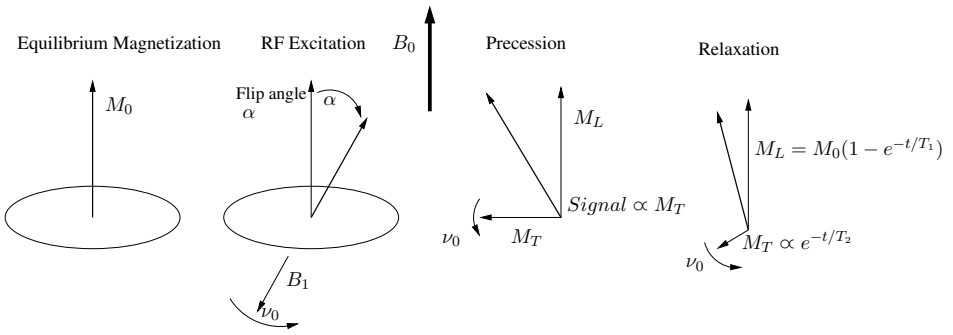

Figure 3.1: The basic physics of the NMR experiment: in a magnetic field $\mathbf{B}_0$, an equilibrium magnetization M_0 forms due to the alignment of nuclear dipoles (left). An RF pulse tips over M_0 creating a longitudinal component M_L and a transverse component M_T (middle). M_T precesses around the direction of $\mathbf{B}_0$, generating a detectable MR signal. Over time M_T decays to zero with a relaxation time T_2 and M_L returns to M_0 with a relaxation time T_1(right). This picture is taken from [4].

with a time constant T_2 while the longitudinal moment M_L reaches its equilibrium with a time constant T_1. The values of M_L and M_T are measured using coils. T_1 and T_2 depend on the environment, so that their local value can be used to discriminate between the tissues, proton density being a third signature to discriminate between tissues. An illustration of the phenomenon is given in figure 3.1.

Measuring M_L (resp. M_T) leads to T_1- (resp. T_2-) weighted images. A subtle but important variant of the T_2 technique is called T_2* imaging. In order to obtain an image, RF pulses are applied repeatedly: such a repetition is called a pulse sequence. Many kinds of pulse sequences are possible, and the sensitivity of the MR images to the different parameters can be adjusted by tuning the repetition time (TR) between consecutive pulses and the time between the RF pulse and the measurement TE (time to echo). Typical sequences may be of several kinds:

- The Gradient Echo Pulse Sequence simply consists of the repetition of the FID described previously. It is simply described by the value of the flip angle α and the repetition time TR.
- The Spin Echo Pulse Sequence consists in applying a first 90 degrees pulse, then after a time TE/2 a 180 degrees pulse in the transverse plane. The effect of this pulse is to refocus the signal whose phase has been quickly dispersed by local field inhomogeneities. Thus, an echo of signal appears at time TE and is measured. This echo can be repeated many times to sample the T_2 decay.
- The Inversion Recovery Pulse Sequence begins with a 180 degrees pulse and after a delay TI a 90 degrees pulse. It enhances the T_1 weighting of the image.

3.1.2 MRI scanning

To selectively image different voxels (picture elements) of a subject, magnetic gradients are applied. Because of the relation (3.1), the spatial variation of the magnetic

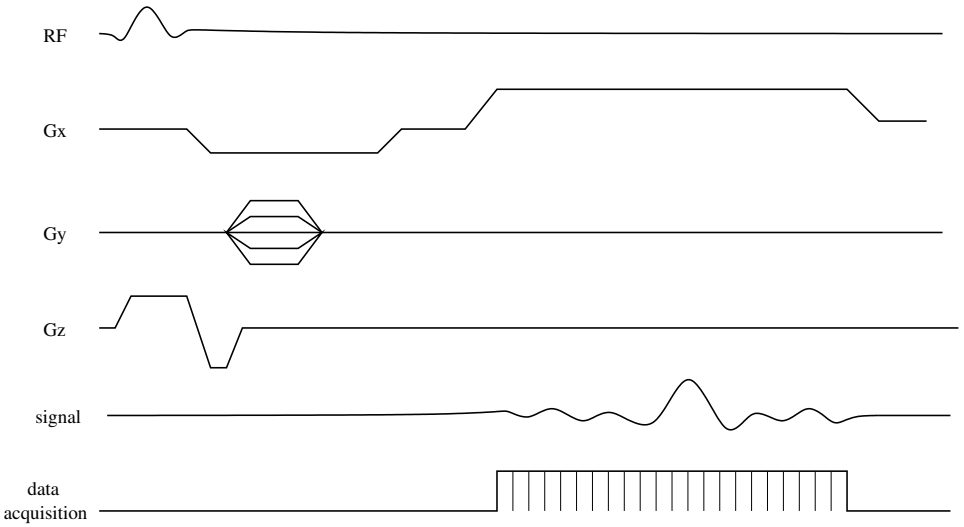

Figure 3.2: A basic imaging pulse sequence.
During the RF excitation pulse a gradient in z is applied (slice selection), and during read-out of the signal a gradient in x is applied (frequency encoding). Between these gradient pulses, a gradient pulse in y is applied, and the amplitude of this pulse is stepped through a different value each time the pulse is repeated (phase encoding). Typically 128 or 256 phase-encoding steps (repeats of the pulse sequence) are required to collect sufficient information to reconstruct an image. This figure is taken from [4].

field magnitude induces a Larmor frequency variation which can be used to localize the piece of material that generated it. Gradients are typically applied during the RF pulses, during the recording of the generated signal and between these two time instants to encode a slice selection, and a position in the slice with a frequency and a phase (see figure 3.2). The same coils are used for the transmission of gradients and the reception of the signal. Since a coil typically encompasses the body (the head of the subject), it measures a sum of the signals from each tissue in the head.

More precisely, the sequence of events that occurs is:

- The magnetic field $\mathbf{B}_0$ is added with a gradient in the z direction. The selection of a particular frequency at the receiver part is then equivalent to the selection of a slice -a plane with a thickness of typically 1 to 10 mm- along the z direction. This procedure is called the *slice selection*.

- Then, within each slice or plane spanned by the resulting directions (x and y), two gradients are applied during the relaxation.

  - In the x direction, a negative gradient is applied after the RF pulse, and a positive one during acquisition, which creates a gradient echo during data acquisition, halfway through the second gradient pulse; The effect is that the precession frequency varies along the x axis, so that a Fourier

transform of the signal gives its amplitude along the axis. This procedure is called *frequency encoding*.

– In the remaining y direction, a gradient field is applied for a short interval between the RF pulse and data acquisition. After cancellation of this field, the precession is at the uniform frequency, but with a phase shift determined by the position on y. Repeating the frequency encoding many times with different phase shifts creates information on the y position. This third procedure is known as *phase encoding*.

For a Repetition Time TR of about 1s, acquiring a single 256×256 slice (which needs 256 phase encoding steps so 256 RF pulses) would require 256s (4min and 16s). Acquiring a full volume like in such a way is impractical. Fortunately, there is a lot of "dead time" in a TR time slice. This "dead time" can be used to acquire several slices in parallel leading to much more reasonnable whole head acquisition times. The amount of slices that can be acquired in parallel as well as the exact gradient patterns that have to be applied can vary. Theses parameters can be tuned to optimize various aspects (acquisition time, contrast, resolution, ...). Designing pulse sequences for a given effect is a complicated task, which is achieved by specialists.

After acquisition of the data in the frequency space, also known as $k-$space, the data is mapped into the 3D space by Fourier transform.

3.2 Segmentation of Magnetic Resonance Images (MRI)

3.2.1 Region labelling

3.2.2 Segmentation

Chapter 4

Forward problem computation

4.1 Introduction

The forward problem of magneto-electro-encephalography aims at computing the electromagnetic field produced by a known primary current, in a known geometry.

This chapter is organized in increasing model complexity. Section 4.2 presents the forward problem in simple geometrical settings for which the calculations can be done by hand. Section 4.3 considers more general nested surface models, which we call "semi-realistic", in which subject-dependent surfaces are designed to match the main tissue interfaces in the head. Computations in the semi-realistic setting are performed using Boundary Element Methods (BEM). Finally, Section 4.4 presents the most sophisticated model, which we call "realistic", which models the tissue conductivity voxel-wise, does not necessitate to define interfaces between tissues of homogeneous conductivity, and allows for tensor-valued conductivity.

4.2 Simple geometries

4.2.1 Current dipole in infinite homogeneous medium

Electrical potential

A current dipole with moment $\mathbf{q}$ and position $\mathbf{p}$ is represented by $\mathbf{J}^{\mathrm{p}}(\mathbf{r}) = \mathbf{q}\,\delta_{\mathbf{p}}(\mathbf{r})$. The potential created by such a dipole follows the Poisson equation

$$\nabla \cdot (\sigma \nabla V) = \mathbf{q} \cdot \nabla \delta(\mathbf{r} - \mathbf{p}) \ .$$

As the medium is infinite with constant conductivity σ,

$$\sigma \Delta V = \mathbf{q} \cdot \nabla \delta(\mathbf{r} - \mathbf{p}) \ .$$

As detailed in Appendix **??**, in three dimensions, the fundamental solution to the Laplacian is $\frac{-1}{4\pi\|\mathbf{r}\|}$ in the sense that

$$\Delta\left(\frac{-1}{4\pi\|\mathbf{r}\|}\right) = \delta_0 \ .$$

Hence,

$$V(\mathbf{r}) = -\frac{1}{4\pi\sigma}\int \mathbf{q}\cdot\nabla'\delta(\mathbf{r}'-\mathbf{p})\frac{1}{\|\mathbf{r}-\mathbf{r}'\|}d\mathbf{r}' = \frac{1}{4\pi\sigma}\mathbf{q}\cdot\frac{\mathbf{r}-\mathbf{p}}{\|\mathbf{r}-\mathbf{p}\|^3} \ .$$

Magnetic field

In an infinite, homogeneous domain, only the primary current contributes to the magnetic field as wass shown in the derivation of 2.19, therefore, for a dipolar source,

$$\mathbf{B} = \frac{\mu_0}{4\pi}\mathbf{q}\times\frac{\mathbf{r}-\mathbf{p}}{\|\mathbf{r}-\mathbf{p}\|^3} \ .$$

4.2.2 Silent sources

Helmholtz, in 1853, was the first to point out the existence of sources which are electromagnetically silent, i.e. produce a null electro-magnetic field. First note that a solenoidal source, such that $\nabla\cdot\mathbf{J}^{\mathrm{p}} = 0$, is electrically silent, since the source term of the Poisson equation vanishes in this case.

Next, we exhibit an electromagnetically silent source, in the form of a primary current $\mathbf{J}^{\mathrm{p}}$, supported on a surface S, and such that $\mathbf{J}^{\mathrm{p}} = q\,\mathbf{n}$ where $\mathbf{n}$ is the normal vector to S and q is a constant. We prove that $\mathbf{J}^{\mathrm{p}}$ is electromagnetically silent if the medium is infinite and homogeneous. We will extend this result to more general domains in the course of this chapter.

In an infinite homogeneous medium the potential V can be written as an integral over the support of the primary current:

$$V(\mathbf{r}) = -\frac{1}{4\pi\sigma}\int \nabla'\cdot\mathbf{J}^{\mathrm{p}}(\mathbf{r}')\frac{1}{\|\mathbf{r}-\mathbf{r}'\|}\,d\mathbf{r}' = \frac{1}{4\pi\sigma}\int \mathbf{J}^{\mathrm{p}}(\mathbf{r}')\cdot\frac{\mathbf{r}-\mathbf{r}'}{\|\mathbf{r}-\mathbf{r}'\|^3}\,d\mathbf{r}' \ .$$

For the particular case of $\mathbf{J}^{\mathrm{p}} = q\,\mathbf{n}\,\delta_S$,

$$V(\mathbf{r}) = \frac{1}{4\pi\sigma}\int_S q\mathbf{n}\cdot\frac{\mathbf{r}-\mathbf{r}'}{\|\mathbf{r}-\mathbf{r}'\|^3}ds = \frac{q}{4\pi\sigma}\int_S \frac{\mathbf{r}-\mathbf{r}'}{\|\mathbf{r}-\mathbf{r}'\|^3}\cdot\mathbf{n}ds$$

The integral on the right represents the solid angle of S viewed from $\mathbf{r}$, and vanishes if $\mathbf{r}$ is exterior to S.

The magnetic field can be represented by the Biot-Savart equation, yielding, if Ω_S denotes the volume contained inside S:

$$\mathbf{B}(\mathbf{r}) = \frac{\mu_0}{4\pi}\int_S q\,\mathbf{n}\times\nabla'\left(\frac{1}{\|\mathbf{r}-\mathbf{r}'\|}\right)ds = \frac{\mu_0\,q}{4\pi}\int_{\Omega_S}\nabla'\times\left(\nabla'\frac{1}{\|\mathbf{r}-\mathbf{r}'\|}\right)d\mathbf{r}' = 0 \ .$$

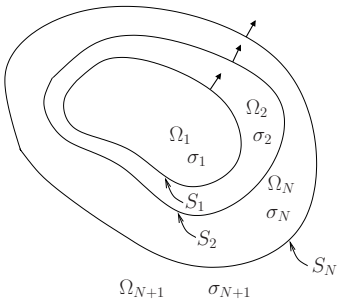

Figure 4.1: The head is modeled as a set of nested regions $\Omega_1, \ldots, \Omega_{N+1}$ with constant isotropic conductivities $\sigma_1, \ldots, \sigma_{N+1}$, separated by interfaces $S_1, \ldots, S_N$. Arrows indicate the normal directions (outward).

4.3 Semi-realistic model

In an infinite, homogeneous domain, the electric potential and the magnetic field decay at the same rate. However, when measured on the scalp, the two fields have very different spatial properties: the magnetic field apears more "focal", and the electric potential more "diffuse". The main reason for this qualitative difference is that the magnetic field is less sensitive than the electric potential to conductivity differences in the tissues of the head. The electric potential, in particular, is subject to diffusion because of the low conductivity of the skull.

In this section, we will consider a piecewise-constant conductivity, organised in layers, as depicted in Figure 4.1.

4.3.1 Magnetic field computation

Section 2.2.2 has established the Biot and Savart law, decomposing the magnetic field into a primary current contribution and an ohmic contribution

$$\mathbf{B} = \mathbf{B}_0 - \frac{\mu_0}{4\pi} \int \sigma \nabla V \times \frac{\mathbf{r} - \mathbf{r}'}{\|\mathbf{r} - \mathbf{r}'\|^3} \, d\mathbf{r}' \ ,$$

where

$$\mathbf{B}_0 = \frac{\mu_0}{4\pi} \int \mathbf{J}^{\mathrm{p}} \times \frac{\mathbf{r} - \mathbf{r}'}{\|\mathbf{r} - \mathbf{r}'\|^3} \, d\mathbf{r}' \ .$$

With the piecewise-constant conductivity model, the ohmic term can be decomposed as a sum over volumes of constant conductivity:

$$\int \sigma \nabla V \times \frac{\mathbf{r} - \mathbf{r}'}{\|\mathbf{r} - \mathbf{r}'\|^3} \, d\mathbf{r}' = \sum_i \sigma_i \int_{\Omega_i} \nabla V \times \frac{\mathbf{r} - \mathbf{r}'}{\|\mathbf{r} - \mathbf{r}'\|^3} \, d\mathbf{r}' = \sum_i \sigma_i I_i \qquad (4.1)$$

In the above identity, note that the conductivities must not only be assumed constant in each domain Ω_i, but also isotropic, in order to take σ_i out of the integral over Ω_i. The volume integral I_i can be expressed as a surface integral on $\partial\Omega_i = S_{i-1} \cup S_i$. With this in view, we use the Stokes formula, and the identity

$$\nabla \times (V \, \nabla g) = \nabla V \times \nabla g \ .$$

Thus

$$I_i = \int_{\Omega_i} \nabla \times \left(V(\mathbf{r}') \frac{\mathbf{r}-\mathbf{r}'}{\|\mathbf{r}-\mathbf{r}'\|^3} \right) d\mathbf{r}' = \int_{\partial\Omega_i} \mathbf{n} \times V(\mathbf{r}') \frac{\mathbf{r}-\mathbf{r}'}{\|\mathbf{r}-\mathbf{r}'\|^3}\, ds$$
$$= \int_{S_i} \mathbf{n} \times V(\mathbf{r}') \frac{\mathbf{r}-\mathbf{r}'}{\|\mathbf{r}-\mathbf{r}'\|^3}\, ds - \int_{S_{i-1}} \mathbf{n} \times V(\mathbf{r}') \frac{\mathbf{r}-\mathbf{r}'}{\|\mathbf{r}-\mathbf{r}'\|^3}\, ds$$

This expression is then inserted in (4.1) and, recalling that $\sigma_{N+1} = 0$,

$$\mathbf{B}(\mathbf{r}) = \mathbf{B}_0(\mathbf{r}) + \frac{\mu_0}{4\pi} \sum_{i=1}^{N} (\sigma_i - \sigma_{i+1}) \int_{S_i} V(\mathbf{r}') \frac{\mathbf{r}-\mathbf{r}'}{\|\mathbf{r}-\mathbf{r}'\|^3} \times \mathbf{n}\, ds \tag{4.2}$$

In the case where the surfaces S_i are spherical, and concentric, the above expression shows that the radial component of the magnetic field is independent of the conductivity profile:

$$\mathbf{B}(\mathbf{r}) \cdot \mathbf{r} = \mathbf{B}_0(\mathbf{r}) \cdot \mathbf{r} \ .$$

This results from the identity

$$((\mathbf{r}-\mathbf{r}') \times \mathbf{r}') \cdot \mathbf{r} = 0 \ .$$

In a spherical geometry, the independence to the conductivity profile can be extended to the three components of the magnetic field, if the source is a single dipole. Indeed, outside Ω, since $\sigma = 0$ and $\mathbf{J}^{\mathrm{p}} = 0$, $\mathbf{J} = 0$ and hence $\nabla \times \mathbf{B} = 0$. The magnetic field thus derives from a "potential" which we denote U:

$$\mathbf{B} = -\nabla U$$

The potential U is only defined up to a constant, but since $\mathbf{B} \to 0$ at infinity, we adjust the constant so that $U \to 0$ at infinity.
Suppose the dipolar source to be located ar $\mathbf{r}_0$, with dipolar moment $\mathbf{q}$. Denote $e_r = \mathbf{r}/\|\mathbf{r}\|$ the unit radial vector. For $\mathbf{r}$ outside Ω,

$$U(\mathbf{r}) = -\int_0^\infty \nabla U(\mathbf{r} + t\, e_r) \cdot e_r\, dt$$
$$= \int_0^\infty \mathbf{B}(\mathbf{r} + t\, e_r) \cdot e_r\, dt = \int_0^\infty \mathbf{B}_0(\mathbf{r} + t\, e_r) \cdot e_r\, dt$$
$$= \frac{\mu_o}{4\pi} \mathbf{q} \times (\mathbf{r} - \mathbf{r}_0) \cdot e_r \int_0^\infty \frac{dt}{\|\mathbf{r} + t\, e_r - \mathbf{r}_0\|^3}$$

The above expression shows that $\mathbf{B}$ is independent of σ. Moreover, for a radial dipole, $\mathbf{q} \times (\mathbf{r} - \mathbf{r}_0) \cdot e_r = 0$, hence $U(\mathbf{r}) = 0$ and $\mathbf{B}(\mathbf{r})$ vanishes outside Ω.

4.3.2 Electric potential computation

The geometrical setting is again the one of Figure 4.1. In each domain Ω_i, the potential follows a Poisson equation

$$\sigma_i \Delta V = f_i$$

where f_i is the restriction of $\nabla \cdot \mathbf{J}^{\mathrm{p}}$ to Ω_i. At the interface S_i between Ω_i and Ω_{i+1}, the following jump conditions hold:

$$[V]_{S_i} = 0 \tag{4.3}$$
$$[\sigma \partial_{\mathbf{n}} V]_{S_i} = 0 \ . \tag{4.4}$$

We define the jump of a function $f : \mathbb{R}^3 \to \mathbb{R}$ at interface S_j as

$$[f]_j = f^-_{S_j} - f^+_{S_j},$$

the functions f^- and f^+ on S_j being respectively the interior and exterior limits of f:

$$\text{for } \mathbf{r} \in S_j, \qquad f^{\pm}_{S_j}(\mathbf{r}) = \lim_{\alpha \to 0^{\pm}} f(\mathbf{r} + \alpha \mathbf{n}).$$

Note that these quantities depend on the orientation of $\mathbf{n}$.

Using the same type of technique as for the magnetic field, one can show that the values of the potential (and of the normal current flow) on surfaces S_i are related by integral operators.

Green formula

We recall the Green formula

$$\int_\Omega (u\,\Delta v - v\,\Delta u)\,d\mathbf{r}' = \int_{\partial\Omega} (u \partial_{\mathbf{n}'} v - v \partial_{\mathbf{n}'} u)\,ds(\mathbf{r}') \ .$$

Consider $v = -\frac{1}{4\pi\|\mathbf{r}-\mathbf{r}'\|} = -G(\mathbf{r}-\mathbf{r}')$ and a harmonic function u.

The left-hand side integral $I(\mathbf{r}) = \int_\Omega (u\,\Delta v - v\,\Delta u)\,d\mathbf{r}'$ takes different values according to the position of $\mathbf{r}$ with respect to Ω, as summarized below:

$\mathbf{r} \in \Omega$	$I(\mathbf{r}) = u(\mathbf{r})$
$\mathbf{r} \in \mathbb{R}^3 \backslash \overline{\Omega}$	$I(\mathbf{r}) = 0$
$\mathbf{r} \in \partial\Omega$	$I(\mathbf{r}) = \frac{u^-(\mathbf{r})}{2}$

The first two lines of the above table are trivial to prove, and the third relies on solid angle computations (refer to [15] for the proof). Thus seen from inside,

$$I(\mathbf{r}) = \int_{\partial\Omega} -u^-(\mathbf{r})\,\partial_{\mathbf{n}'} G(\mathbf{r}-\mathbf{r}') + G(\mathbf{r}-\mathbf{r}')\,\partial^-_{\mathbf{n}'}(\mathbf{r}')\,ds(\mathbf{r}') \tag{4.5}$$

The same treatment can be applied to the volume $\Omega' = \mathbb{R}^3 \backslash \overline{\Omega}$, and seen from Ω, this yields

$$J(\mathbf{r}) = \int_{\partial\Omega} u^+(\mathbf{r})\,\partial_{\mathbf{n}'} G(\mathbf{r}-\mathbf{r}') - G(\mathbf{r}-\mathbf{r}')\,\partial^+_{\mathbf{n}'}(\mathbf{r}')\,ds(\mathbf{r}') \tag{4.6}$$

with the integral term $J(\mathbf{r})$ equal to

$\mathbf{r} \in \mathbb{R}^3 \backslash \overline{\Omega}$	$J(\mathbf{r}) = u(\mathbf{r})$
$\mathbf{r} \in \Omega$	$J(\mathbf{r}) = 0$
$\mathbf{r} \in \partial\Omega$	$J(\mathbf{r}) = \frac{u^-(\mathbf{r})}{2}$

Summing (4.5) and (4.6), for $\mathbf{r} \in \Omega$,

$$u(\mathbf{r}) = -\int_{\partial\Omega} [u]\, \partial_{\mathbf{n}'} G(\mathbf{r}-\mathbf{r}') ds(\mathbf{r}') + \int_{\partial\Omega} [\partial_{\mathbf{n}'} u]\, G(\mathbf{r}-\mathbf{r}') ds(\mathbf{r}')$$

and, for $\mathbf{r} \in \partial\Omega$,

$$\frac{u^+(\mathbf{r}) + u^-(\mathbf{r}')}{2} = -\int_{\partial\Omega} [u]\, \partial_{\mathbf{n}'} G(\mathbf{r}-\mathbf{r}') ds(\mathbf{r}') + \int_{\partial\Omega} [\partial_{\mathbf{n}'} u]\, G(\mathbf{r}-\mathbf{r}') ds(\mathbf{r}')$$

To simplify notation, we introduce two integral operators, called the "double-layer" and "single-layer" operators, which map a scalar function f on $\partial\Omega$ to another scalar function on $\partial\Omega$:

$$\begin{aligned} \big(\mathcal{D}f\big)(\mathbf{r}) &= \int_{\partial\Omega} \partial_{\mathbf{n}'} G(\mathbf{r}-\mathbf{r}') f(\mathbf{r}')\, \mathrm{d}s(\mathbf{r}') \\ \big(\mathcal{S}f\big)(\mathbf{r}) &= \int_{\partial\Omega} G(\mathbf{r}-\mathbf{r}') f(\mathbf{r}')\, \mathrm{d}s(\mathbf{r}') \ . \end{aligned}$$

The two above relations become, for $\mathbf{r} \in \Omega$,

$$u(\mathbf{r}) = -\mathcal{D}\,[u] + \mathcal{S}\,[\partial_{\mathbf{n}} u]$$

and for $\mathbf{r} \in \partial\Omega$,

$$u^{\mp}(\mathbf{r}) = \big(\pm\tfrac{I}{2} - \mathcal{D}\big)\,[u] + \mathcal{S}\,[\partial_{\mathbf{n}} u]$$

This also holds when $\Omega = \Omega_1 \cup \Omega_2 \cup \ldots \Omega_N$, with $\partial\Omega = S_1 \cup S_2 \cup \ldots S_N$. In this case, for $\mathbf{r} \in S_i$,

$$\frac{u^-(\mathbf{r}) + u^+(\mathbf{r})}{2} = \textstyle\sum_{j=1}^N -\mathcal{D}_{ij}\,[u]_{S_j} + \mathcal{S}_{ij}\,[\partial_{\mathbf{n}} u]_{S_j} \tag{4.7}$$

Geselowitz formula

Supposing the primary current $\mathbf{J}^{\mathrm{p}}$ to be restricted to one volume Ω_i, consider V_∞ sich that $\sigma_i \Delta V_\infty = \nabla \cdot \mathbf{J}^{\mathrm{p}}$ holds in all $\mathbb{R}^3$. Across each surface S_j, the potential V_∞ and its normal derivative $\partial_{\mathbf{n}} V$ are continuous. Consider the function $u = \sigma\, V - \sigma_i V_\infty$; it is harmonic in each Ω_j, therefore satisfies (4.7). Since $[u]_{S_j} = (\sigma_j - \sigma_{j+1}) V_j$ and $[\partial_{\mathbf{n}} u] = 0$, we obtain, on each surface S_j,

$$\frac{\sigma_j + \sigma_{j+1}}{2} V_j + \sum_{k=1}^{N} (\sigma_k - \sigma_{k+1})\, \mathcal{D}_{jk}\, V_k = \sigma_i V_\infty \ , \tag{4.8}$$

a formula which was established in 1967 by Geselowitz.

4.4 Realistic model

For even more realistic models, the piecewise constancy of conductivity that has been made in the previous section needs to be relaxed. Indeed, the brain is known to have strong anisotropies in the conductivities at least in two domains:

- the skull is a non-homogeneous material. It is a porous material with marrow insertions and all kinds of holes filled with air or various liquids (eg. sinuses). Also, its shape is extremely complex and difficult to extract from MRI images, so that it is often "guessed" by using its relative position with respect to the other interfaces. In practice, researchers have found that its conductivity plays a fundamental role in EEG and that it would best modelled (in absence of more direct measurements) with distinct radial and tangential conductivities.

- the white matter is even less homogeneous: it is made of an entanglement of fibers connecting different pieces of the cortex. It has thus a strong anisotropic behavior. While the importance of taking into account this anisotropy for MEG/EEG reconstruction has less been investigated, it is certainly interesting to evaluate its effects and fortunately, there exists a way of measuring it (contrarily to the case of the skull). Diffusion MRI is able to measure the diffusion of water molecules in various directions. Intuitively, the water flow more easily along the direction of the fibers in the white matter than across them. This anisotropy of diffusion of water can be used to model an anisotropic conductivity as currents are certainly better conducted along the fibers than across them.

Dealing with such anisotropies with a BEM like method is impossible most of the time (it would be possible to deal with radial and tangential anisotropies for a spherical head but not much more). Thus, this problem needs to be tackled using directly the Maxwell equation in the quasistatic case. So we start again with the Poisson equation

$$\nabla \cdot (\sigma \nabla V) = f = \nabla \cdot \mathbf{J}^{\mathrm{p}} \ .$$

To obtain a unique solution, this equation needs to be supplemented with a boundary condition. To do so, we hypothesize that no current flows outside of the head (which is mostly true except at the spinal column which is "far" from most EEG/MEG measurements). We thus have to solve the following problem:

$$\left\{ \begin{array}{rcll} \nabla \cdot (\sigma \nabla V) & = & \nabla \cdot \mathbf{J}^{\mathrm{p}} & \text{in} \quad \Omega \\ \sigma \dfrac{\partial V}{\partial \mathbf{n}} = \sigma \nabla V \cdot \mathbf{n} & = & 0 & \text{on} \quad S = \partial\Omega. \end{array} \right. \tag{4.9}$$

This problem will be solved using a Finite Element Approach. We will first show that the PDE 4.9 can be formulated as a variational problem (section 4.4.1), which is then discretized to obtain a linear system (section 4.4.2), and then solved (section 4.4.3).

Anisotropic model Note that in the above formulation, σ can either be taken as a simple scalar function of $\mathbf{r}$ but it can as well be a function that associates a 3D symmetric definite positive matrix at each point of the space. This matrix is a

tensorial description of the anisotropic conductivity (the eigenvalues represent the conductivity along the corresponding eigenvector). Denoting by $\mathbf{\Sigma}$ this matrix, the anisotropic system becomes:

$$\left\{ \begin{array}{rcll} \nabla \cdot (\mathbf{\Sigma} \nabla V) & = & \nabla \cdot \mathbf{J}^{\mathrm{p}} & \text{in} \quad \Omega \\ \mathbf{\Sigma} \dfrac{\partial V}{\partial \mathbf{n}} = \mathbf{\Sigma} \nabla V \cdot \mathbf{n} & = & 0 & \text{on} \quad S = \partial\Omega. \end{array} \right. \tag{4.10}$$

For simplicity, we will develop the scalar model hereafter but most of the results can be trivially adapted to the anisotropic case. Notationnally, almost nothing changes except that $\sigma(\mathbf{r}) \nabla V(\mathbf{r}) \cdot \nabla w(\mathbf{r})$ is replaced by $\nabla V(\mathbf{r})^T \mathbf{\Sigma} \nabla w(\mathbf{r})$ and $\sigma(\mathbf{r}) \| \nabla \phi(\mathbf{r}) \|^2$ is replaced by $\nabla \phi(\mathbf{r})^T \mathbf{\Sigma} \nabla \phi(\mathbf{r})$.

4.4.1 A variational formulation of the forward problem

Let us first define some functional spaces that will be needed hereafter.

$$H^1(\Omega) = \left\{ w \in L^2(\Omega), \nabla w \in L^2(\Omega)^3 \right\} .$$

$$H^2(\Omega) = \left\{ w \in L^2(\Omega), \nabla w \in H^1(\Omega)^3 \right\} .$$

These spaces provide functions that can be simply plugged within the equations that will be used (with all integrals and differentiations well defined).

We first show that the following three problems are equivalent:

① $V \in H^2(\Omega)$ is solution of:

$$\left\{ \begin{array}{rcll} \nabla \cdot (\sigma \nabla V) & = & f & \text{in} \quad \Omega \\ \sigma \dfrac{\partial V}{\partial \mathbf{n}} = \sigma \nabla V \cdot \mathbf{n} & = & g & \text{on} \quad S = \partial\Omega. \end{array} \right.$$

② $V \in H^1(\Omega)$ is such that

$$\forall w \in H^1(\Omega) \quad \int_\Omega \sigma(\mathbf{r}) \nabla V(\mathbf{r}) \cdot \nabla w(\mathbf{r}) \, d\mathbf{r} + \int_\Omega f(\mathbf{r}) w(\mathbf{r}) \, d\mathbf{r} - \int_S g(\mathbf{r}) w(\mathbf{r}) \, ds = 0 .$$

③ $V = arg \min_{\phi \in H^1(\Omega)} E(\phi)$ with:

$$E(\phi) = \frac{1}{2} \int_\Omega \sigma(\mathbf{r}) \| \nabla \phi(\mathbf{r}) \|^2 \, d\mathbf{r} + \int_\Omega f(\mathbf{r}) \phi(\mathbf{r}) \, d\mathbf{r} \; - \int_S g(\mathbf{r}) \phi(\mathbf{r}) \, ds .$$

Notice that the PDE in ① is exactly the same as the one in 4.9: we have just renamed $f = \nabla \cdot \mathbf{J}^{\mathrm{p}}$ and allowed for a more general Neumann boundary condition g. This makes the presentation slightly more general and shows that the basic method will remain the same even if we were able to model the currents in the neck. The functions f and g are supposed to be square integrable, that is $f \in L^2(\Omega)$ and $g \in L^2(\partial\Omega)$.

Theorem 4.1. *Problems ①, ② and ③ are equivalent.*

Proof. Problem ② will be used as a pivot. The proof is thus in two parts: equivalence of ① and ②, and equivalence of ② and ③.

① $\Longrightarrow$ ②
Using the formula: $\nabla \cdot (\sigma w \nabla V) = \sigma \nabla V \cdot \nabla w + w \nabla \cdot \sigma \nabla V$ and integrating it over the domain Ω, we have:

$$\int_\Omega w(\mathbf{r}) \nabla \cdot \sigma(\mathbf{r}) \nabla V(\mathbf{r})\, d\mathbf{r} = \int_\Omega \nabla \cdot (\sigma(\mathbf{r}) w(\mathbf{r}) \nabla V(\mathbf{r}))\; d\mathbf{r} - \int_\Omega \sigma(\mathbf{r}) \nabla V(\mathbf{r}) \cdot \nabla w(\mathbf{r})\, d\mathbf{r}$$

In the left hand side of this equation, $\nabla \cdot \sigma \nabla V$ can be replaced by f because of ①. The Green theorem can be used to transform the first term of the right hand side giving:

$$\int_\Omega \sigma(\mathbf{r}) \nabla V(\mathbf{r}) \cdot \nabla w(\mathbf{r})\, d\mathbf{r} + \int_\Omega f(\mathbf{r}) w(\mathbf{r})\, d\mathbf{r} - \int_S w(\mathbf{r}) \sigma(\mathbf{r}) \nabla V(\mathbf{r}) \cdot \mathbf{n}\, ds = 0\ .$$

Replacing $\sigma(\mathbf{r}) \nabla V(\mathbf{r}) \cdot \mathbf{n}$ by its value on S as given by the boundary condition of ① yields the result.

$$\int_\Omega \sigma(\mathbf{r}) \nabla V(\mathbf{r}) \cdot \nabla w(\mathbf{r})\, d\mathbf{r} + \int_\Omega f(\mathbf{r}) w(\mathbf{r})\, d\mathbf{r} - \int_S g(\mathbf{r}) w(\mathbf{r})\, ds = 0\ .$$

② $\Longrightarrow$ ①
If ② is true for any $w \in H^1(\Omega)$, it is also true for $w \in D(\Omega)$ the space of C^∞ functions with compact support in Ω. The dual of $D(\Omega)$ is the space of distributions over Ω, $D'(\Omega)$. If $\nabla \cdot (\sigma \nabla V) \in L^2(\Omega)$, then $\nabla \cdot (\sigma \nabla V) - f \in L^2(\Omega)$ since $f \in L^2(\Omega)$ by hypothesis. Denoting by $< \ldots >$ the duality bracket between the spaces $L^2(\Omega)$ and $D'(\Omega)$. Thus Eq. ② can be written as $< \nabla \cdot (\sigma \nabla V) - f, w >= 0$. From a standard result in functional analysis [Brezis 88], $\nabla \cdot (\sigma \nabla V) - f$ is zero almost everywhere.

③ $\Longrightarrow$ ②
If ③ is true, then for all $w \in H^1(\Omega)$ and for any real number λ, we have:

$$E(V) \leq E(V + \lambda w)\ . \tag{4.11}$$

This is true because:

$$\forall V \in H^2(\Omega) \quad \forall w \in H^1(\Omega) \quad \forall \lambda \in \mathbb{R} \quad V + \lambda w \in H^1(\Omega)$$

By definition of E:

$$\begin{aligned} E(V+\lambda w) &= \frac{1}{2}\int_\Omega \sigma(\mathbf{r})\|\nabla(V+\lambda w)(\mathbf{r})\|^2\,d\mathbf{r} + \int_\Omega f(\mathbf{r})(V+\lambda w)(\mathbf{r})\,d\mathbf{r} - \\ &\quad \int_S g(\mathbf{r})(V+\lambda w)(\mathbf{r})\,ds \\ &= \frac{1}{2}\int_\Omega \sigma(\mathbf{r})\|\nabla V(\mathbf{r})\|^2\,d\mathbf{r} + \int_\Omega f(\mathbf{r})V(\mathbf{r})\,d\mathbf{r} - \int_S g(\mathbf{r})V(\mathbf{r})\,ds + \\ &\quad \lambda\int_\Omega \sigma(\mathbf{r})\nabla V(\mathbf{r})\cdot\nabla w(\mathbf{r})\,d\mathbf{r} + \lambda\int_\Omega f(\mathbf{r})w(\mathbf{r})\,d\mathbf{r} - \lambda\int_S g(\mathbf{r})w(\mathbf{r})\,ds + \\ &\quad \frac{\lambda^2}{2}\int_\Omega \sigma(\mathbf{r})\|\nabla w(\mathbf{r})\|^2\,d\mathbf{r}\,. \end{aligned} \tag{4.12}$$

$$\begin{aligned} E(V+\lambda w) &= E(V) + \frac{\lambda^2}{2}\int_\Omega \sigma(\mathbf{r})\|\nabla w(\mathbf{r})\|^2\,d\mathbf{r} \\ &\quad \lambda\left(\int_\Omega \sigma(\mathbf{r})\nabla V(\mathbf{r})\cdot\nabla w(\mathbf{r})\,d\mathbf{r} + \int_\Omega f(\mathbf{r})w(\mathbf{r})\,d\mathbf{r} - \int_S g(\mathbf{r})w(\mathbf{r})\,ds\right) \end{aligned} \tag{4.13}$$

For λ sufficiently small and positive, Eq. 4.11 implies:

$$\int_\Omega \sigma(\mathbf{r})\nabla V(\mathbf{r})\cdot\nabla w(\mathbf{r})\,d\mathbf{r} + \int_\Omega f(\mathbf{r})w(\mathbf{r})\,d\mathbf{r} - \int_S g(\mathbf{r})w(\mathbf{r})\,ds \geq 0\,.$$

For λ sufficiently small and negative, Eq. 4.11 implies:

$$\int_\Omega \sigma(\mathbf{r})\nabla V(\mathbf{r})\cdot\nabla w(\mathbf{r})\,d\mathbf{r} + \int_\Omega f(\mathbf{r})w(\mathbf{r})\,d\mathbf{r} - \int_S g(\mathbf{r})w(\mathbf{r})\,ds \leq 0\,.$$

Thus:

$$\int_\Omega \sigma(\mathbf{r})\nabla V(\mathbf{r})\cdot\nabla w(\mathbf{r})\,d\mathbf{r} + \int_\Omega f(\mathbf{r})w(\mathbf{r})\,d\mathbf{r} - \int_S g(\mathbf{r})w(\mathbf{r})\,ds = 0\,.$$

② $\Longrightarrow$ ③
From Eq. 4.13 with ②, denoting by ϕ the value $V+\lambda w$, it is clear that $E(V)$ is the minimum value of $E(\phi)$. This is true since when w spans $H^1(\Omega)$ and for all real λ, $\phi = V+\lambda w$ spans $H^1(\Omega)$.

□

4.4.2 Discretization of the FEM forward problem

General discrete framework

The FEM forward problem is implemented using the variational formulation ③. The continuous functional spaces are approximated using the Galerkin method (see section **??**) yielding a discrete problem.

The 3D space Ω is tessellated with bounded cells (eg tetrahedra or hexahedra) (C_i), $i = 1 \ldots N_C$. This tessellation Ω_h also introduces a set of points (V_i), $i =$

$1 \dots N_V$ (the vertices of the cells) and the space of the continuous functions over Ω is approximated by a vector space using some basis functions (w^i), $i = 1 \dots N_V$ defined at each vertex.

$$H_h^1(\Omega_h) = \left\{ \phi_h, \exists(\phi_1, \dots, \phi_{N_V}) \in \mathbb{R}^{N_V}, \quad \phi_h(\mathbf{r}) = \sum_{i=1}^{N_V} \phi_i w^i(\mathbf{r}) \right\} ,$$

The boundary of the tessellation S_h also defines a tessellation of S the boundary of Ω. Without loss of generality, we assume that the vertices of the tessellation that are on the boundary of the tessellation are (V_i), $i = 1 \dots N_S$ with $N_S < N_V$.

$$H_h^1(S_h) = \left\{ \phi_h, \exists(\phi_1, \dots, \phi_{N_S}) \in \mathbb{R}^{N_S}, \quad \phi_h(\mathbf{r}) = \sum_{i=1}^{N_S} \phi_i w^i_{S_h}(\mathbf{r}) \right\} ,$$

where $w^i_{S_h}$ is the restriction to S_h of the function w^i.

The discretization of the criterion E in ③ is obtained by using the discretized versions of all the involved functions ϕ, f and g. For σ, we will use a different dicretization scheme where σ is given by a constant σ_i over the cell C_i.

$$\begin{aligned} E(\phi_h) &= \frac{1}{2} \int_\Omega \sigma(\mathbf{r}) \left\| \nabla \left(\sum_{i=1}^{N_V} \phi_i w^i(\mathbf{r}) \right) \right\|^2 d\mathbf{r} + \int_\Omega f(\mathbf{r}) \left(\sum_{i=1}^{N_V} \phi_i w^i(\mathbf{r}) \right) d\mathbf{r} \; - \\ &\quad \int_S \left(\sum_{i=1}^{N_V} \phi_i w^i_{S_h}(\mathbf{r}) \right) g(\mathbf{r}) \, ds \\ &= E_h(\Phi) , \end{aligned}$$

where $\Phi = (\phi_1, \dots, \phi_{N_V}) \in \mathbb{R}^{N_V}$.

$$E_h(\Phi) = \frac{1}{2} \sum_{i,j=1}^{N_V} \phi_i \phi_j \int_\Omega \sigma(\mathbf{r}) \nabla w^i(\mathbf{r}) \cdot \nabla w^j(\mathbf{r}) \, d\mathbf{r} + \sum_{i=1}^{N_V} \phi_i \int_\Omega f(\mathbf{r}) w^i(\mathbf{r}) \, d\mathbf{r} - \sum_{i=1}^{N_S} \phi_i \int_S w^i_{S_h}(\mathbf{r}) g(\mathbf{r}) \, ds$$

The minimization of $E(\phi)$ then becomes a simple problem of minimizing in finite dimension the quadratic criterion $E_h(\Phi)$. Denoting by A_{ij} the second order derivative of this criterion $\frac{\partial^2 E_h}{\partial \phi_i \partial \phi_j}$, we have:

$$A_{ij} = \int_\Omega \sigma(\mathbf{r}) \nabla w^i(\mathbf{r}) \cdot \nabla w^j(\mathbf{r}) \, d\mathbf{r} .$$

Note that the matrix $\mathbf{A}$ is naturally symmetric. We also introduce the vector $\mathbf{B}$:

$$B_i = \begin{cases} \int_\Omega f(\mathbf{r}) w^i(\mathbf{r}) \, d\mathbf{r} - \int_S w^i_{S_h}(\mathbf{r}) g(\mathbf{r}) \, ds & \text{for } i \leq N_S \\ \int_\Omega f(\mathbf{r}) w^i(\mathbf{r}) \, d\mathbf{r} & \text{otherwise .} \end{cases}$$

The criterion $E_h(\Phi)$ can be written as $\frac{1}{2} \Phi^T \mathbf{A} \Phi + \mathbf{B} \cdot \Phi$ and optimality is obtained when $\mathbf{A}\Phi + \mathbf{B} = 0$.

$$\Phi^T \mathbf{A} \Phi = \sum_{i,j=1}^{N_V} \phi_i \phi_j A_{ij} = \sum_{i,j=1}^{N_V} \int_\Omega \phi_i \phi_j \sigma(\mathbf{r}) \nabla w^i(\mathbf{r}) \cdot \nabla w^j(\mathbf{r}) \, d\mathbf{r} = \int_\Omega \sigma(\mathbf{r}) \left\| \nabla \phi_h(\mathbf{r}) \right\|^2 d\mathbf{r} \tag{4.14}$$

This proves that the matrix $\mathbf{A}$ is positive because $\sigma > 0$ over Ω. Note, however that the matrix is not definite. Indeed, $\Phi^T\mathbf{A}\Phi$ is zero iff $\nabla\phi_h(\mathbf{r}) = 0$ on Ω almost everywhere. This is natural as the original equation is insensitive to the addition to V of a constant function over Ω. On our discretized spaces, this happens for $\Phi = Cst\mathbf{1}$ (this is the case whenever the constant function over Ω_h belongs the space $H_h^1(\Omega_h)$ which is the case for the standard basis functions P^1 or Q^1 used for tetrahedric or hexahedric cells respectively). Similarly to Eq. 4.14, we can prove that $\Phi^T\mathbf{A}\Psi = \int_\Omega \sigma(\mathbf{r})\nabla\phi_h(\mathbf{r}) \cdot \nabla\psi_h(\mathbf{r})\, d\mathbf{r}$. Applying this result to $\Psi = \mathbf{1}$, proves that the kernel of the matrix $\mathbf{A}$ is the constant vector $\mathbf{1}$. Rewriting this result for each line of the matrix gives:

$$\forall i = 1 \dots N_V \quad \sum_{j=1}^{N_V} A_{ij} = 0 \; . \tag{4.15}$$

This result can be used to reduce the amount of memory used to store the matrix $\mathbf{A}$. Indeed, Eq 4.15 can be rewritten as:

$$A_{ii} = -\sum_{j \neq i} A_{ij} \; . \tag{4.16}$$

This can be used to rewrite conveniently the part of the criterion $E(\phi_h)$ containing $\mathbf{A}$.

$$C(\Phi) = \frac{1}{2}\Phi^T\mathbf{A}\Phi = \frac{1}{2}\sum_{i,j=1}^{N_V} \phi_i\phi_j A_{ij} = \frac{1}{2}\sum_{i=1}^{N_V} A_{ii}\phi_i^2 + \frac{1}{2}\sum_{i \neq j} A_{ij}\phi_i\phi_j \; .$$

Replacing A_{ii} by its value given by Eq. 4.16 yields:

$$\begin{aligned}
C(\Phi) &= \frac{1}{2}\sum_{i=1}^{N_V}\sum_{i \neq j}\left(-A_{ij}\phi_i^2 + A_{ij}\phi_i\phi_j\right) \\
&= \frac{1}{2}\sum_{i=1}^{N_V}\sum_{i \neq j} A_{ij}\left(\phi_j - \phi_i\right)\phi_i \\
&= \frac{1}{2}\sum_{i=1}^{N_V}\sum_{i < j} A_{ij}\left[\left(\phi_j - \phi_i\right)\phi_i + \left(\phi_j - \phi_i\right)\phi_i\right] \quad \text{since} A_{ji} = A_{ij} \\
&= -\frac{1}{2}\sum_{i=1}^{N_V}\sum_{i < j} A_{ij}\left(\phi_j - \phi_i\right)^2
\end{aligned}$$

This formulation has a double advantage:

- it totally removes the need for the terms A_{ii} which do not need to be computed nor stored.
- if we recall that ϕ_h represents a potential, the criterion explicitly involves the differences of these potential values. This is physically very natural.

A P^1 implementation

In practice, we will use P^1 basis function over a tetrahedral mesh. In dimension d, a tetrahedron T_j is defined by $d+1$ vertices $\mathbf{V}_{i_k}, k = 1 \dots d+1$. The restriction w_j^i of w^i to T_j is defined by (for notational simplicity, we assume without loss of generality that $\mathbf{V}_{i_1} = \mathbf{V}_i$):

$$w_j^i(\mathbf{r}) = \begin{cases} 0 & \text{if the vertex } \mathbf{V}_i \text{ does not belong to } T_j \\ \frac{|\mathbf{r}\, \mathbf{V}_2 \dots \mathbf{V}_{d+1}|}{|\mathbf{V}_1 \dots \mathbf{V}_{d+1}|} & \text{otherwise} , \end{cases}$$

where the vectors in the determinants are written with $d+1$ coordinates: the usual d coordinates are augmented with a final 1 (this is called projective or homogeneous coordinates). Because w_j^i is a linear function of $\mathbf{r}$, its gradient is a constant vector which can be computed as the first row of the inverse matrix $[\mathbf{V}_1 - \mathbf{V}_{d+1} \dots \mathbf{V}_d - \mathbf{V}_{d+1}]^{-1}$. Given this value of the gradient ∇w_j^i, the matrix $\mathbf{A}$ is computed as:

$$A_{ij} = \sum_{k:\mathbf{V}_i \in T_k, \mathbf{V}_j \in T_k} \int_{T_k} \sigma_k \nabla w_k^i \cdot \nabla w_k^j(\mathbf{r})\, d\mathbf{r} ,$$

This shows that the only non-diagonal (since diagonal elements do not need to be computed) non-zero coefficients of the matrix $\mathbf{A}$ correspond to the edges of the mesh. Consequently, the matrix $\mathbf{A}$ is very sparse.

Since we usually assume that $g = 0$ for the forward problem, the computation of $\mathbf{B}$ includes only the term containing $f = \nabla \cdot \mathbf{J}^{\mathrm{p}}$.

$B_i = \int_\Omega \nabla \cdot \mathbf{J}^{\mathrm{p}}(\mathbf{r}) w^i(\mathbf{r}) d\mathbf{r}$ becomes:

$$\begin{aligned} B_i &= \int_\Omega \nabla \cdot \left(w^i(\mathbf{r}) \mathbf{J}^{\mathrm{p}}(\mathbf{r}) \right) d\mathbf{r} - \int_\Omega \nabla w^i(\mathbf{r}) \cdot \mathbf{J}^{\mathrm{p}}(\mathbf{r})\, d\mathbf{r} \\ &= \int_S w^i(\mathbf{r}) \mathbf{J}^{\mathrm{p}}(\mathbf{r}) \cdot\, ds(\mathbf{r}) - \int_\Omega \nabla w^i(\mathbf{r}) \cdot \mathbf{J}^{\mathrm{p}}(\mathbf{r})\, d\mathbf{r} \\ &= \int_S w^i(\mathbf{r}) \mathbf{J}^{\mathrm{p}}(\mathbf{r}) \cdot \mathbf{n}(\mathbf{r})\, ds(\mathbf{r}) - \int_\Omega \nabla w^i(\mathbf{r}) \cdot \mathbf{J}^{\mathrm{p}}(\mathbf{r})\, d\mathbf{r} \end{aligned}$$

To go further, one needs to choose a proper model for $\mathbf{J}^{\mathrm{p}}$.

The continuous case In this first case, $\mathbf{J}^{\mathrm{p}}$ is represented as $\mathbf{J}^{\mathrm{p}}(\mathbf{r}) = \sum_{j=1}^{N_V} w^j(\mathbf{r}) \mathbf{J}_j^{\mathrm{p}}$. Consequently:

$$B_i = \sum_{j=1}^{N_V} \mathbf{J}_j^{\mathrm{p}} \int_S w^i(\mathbf{r}) w^j(\mathbf{r}) ds(\mathbf{r}) - \sum_{j=1}^{N_V} \mathbf{J}_j^{\mathrm{p}} \int_\Omega \nabla w^i(\mathbf{r}) \cdot w^j(\mathbf{r}) d\mathbf{r}$$

Assuming that there are no sources on S gives:

$$B_i = \sum_{j=1}^{N_V} \mathbf{J}_j^{\mathrm{p}} \int_\Omega \nabla w^i(\mathbf{r}) \cdot w^j(\mathbf{r}) d\mathbf{r}$$

The Dirac case In this case, the current distribution is localized at a single point in space $\mathbf{r}_0$ (or at a few places by linear combination). At this point in space the current orientation and strength are described by a vector μ. Thus, $\mathbf{J}^{\mathrm{p}}(\mathbf{r})$ can be written as: $\mathbf{J}^{\mathrm{p}}(\mathbf{r}) = \mu\delta(\mathbf{r} - \mathbf{r}_0)$. Consequently,

$$B_i = \mu \int_S w^i(\mathbf{r})\delta(\mathbf{r} - \mathbf{r}_0)d\mathbf{r} - \mu \cdot \nabla w^i(\mathbf{r}_0)$$

Assuming again that there are no sources on S gives:

$$B_i = -\mu \cdot \nabla w^i(\mathbf{r}_0)$$

4.4.3 Solving the FEM forward problem

The discretized problem solution can be found by solving $\mathbf{AV} + \mathbf{B} = \mathbf{0}$. This is a fairly simple matrix problem, which could in theory be solved using a pseudo-inverse (the inverse of $\mathbf{A}$ does not exist since its kernel is the vector $\mathbf{1}$). However, $\mathbf{A}$ is a very big matrix which can be stored only because it is sparse. Since the pseudo-inverse (or the inverse) of a sparse matrix is usually not a sparse matrix, it is unwise to try to compute it, as the amount of memory needed to store it will be huge. It is thus a much better idea to solve $\mathbf{AV} + \mathbf{B} = \mathbf{0}$ using an iterative method for each $\mathbf{B}$. Since the matrix $\mathbf{A}$ is symmetric and positive, the conjugate gradient method can be used. Strictly speaking, this method can only be used with definite matrices, but it actually works in this case provided that $\mathbf{B}$ is in the range of matrix $\mathbf{A}$. Because $\mathbf{A}$ is symmetric, the property (4.15) also holds for column vectors of $\mathbf{A}$, which means that these columns are all orthogonal to the constant vector $\mathbf{1}$. These vectors thus all have the property that their mean value is zero. It can be verified that this property is true for the various versions of $\mathbf{B}$ detailed above.

The conjugate gradient method only needs to evaluate the quantity $\mathbf{g} = \mathbf{A\Phi} + \mathbf{B}$ for any given parameter vector Φ and the quantity $\mathbf{g}^T\mathbf{Ag}$ to compute the optimal step at each iteration. These two quantities can be easily evaluated using simple traversal of all the edges of the mesh.

In general, the conjugate gradient method only requires a few steps to converge (typically one or two magnitude order less iterations than N_V the size of the matrix). However, due to the very different values of the conductivities for the various parts of the head, this leads to badly conditionned matrices $\mathbf{A}$. To improve the speed of converge, it is ths preferable to use a preconditioned conjugate gradient method. A simple diagonal preconditioner is already very effective. Such a preconditioner is obtained by the inverting a diagonal matrix whose entries are the diagonal elements of the matrix $\mathbf{A}$.

Part II

Analysis of functional imaging data

Chapter 5

Functional Magnetic Resonance Imaging

Functional Magnetic Resonance Imaging (fMRI) appeared around 1990-1993 and allows various inferences on how the brain is functioning, such as:

- Localization of the main functional areas.
- Study of the spatio/temporal structure of these activations.
- Synchronisation between various areas.

fMRI studies can be made either in an exploratory mode in which there is little a priori on what should be observed or in an estimation mode where a given known activity is searched for. Typically, an acquisition is a 3D+t signal represented by a sequence of 3D images. For reasons that will be explained later, the spatial resolution is somewhat worse than that of anatomic MRI: currently one can expect to have images with a voxel size of 3mm and a temporal resolution of 3s. This means that currently one can expect to have several hundreds of images in an experimental set.

5.1 Origins of the fMRI signal: the BOLD effect

The origins of the fMRI signal are still not very well understood. MRI machines can be tuned to acquire images that measure different phenomena. We focus here on the Blood Oxygen Level Dependent (BOLD) effect, which is the principal acquisition mode used nowadays.

As skteched in section **??**, brain activity translates into action potentials, which correspond to the depolarization of the neuron membrane, which occurs through the exchange of ions – essentially potassium K^+ and sodium Na^+ (see figure 5.1).

At the level of synapses, this information is exchanged through the release of neurotransmitters that bind to receptor sites on post-synaptic terminals, yielding the next neuron to depolarization. Recovery from neuronal signaling requires uptake and repackaging of neurotransmitter and restoration of ionic gradients, all processes

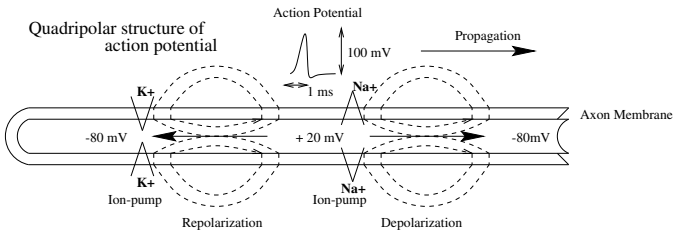

Figure 5.1: The ion exchanges corresponding to action potentials.

that consume Adenosin Triphosphate (ATP). ATP consumption, in turn, requires a continuous supply of glucose and oxygen which is provided by Cerebral Blood Flow (CBF)[1]. It was noticed quite early [12] that brain activity can be assessed by the measurement of regional CBF. These is the effect measured eg with Positron Emission Tomography (PET). The BOLD effect measured by fMRI is more subbtle.

It is important to note that while the oxygenated blood has basically the same magnetic susceptibility as the surrounding brain tissues, deoxyhemoglobin (the deoxygenated hemoglobin) is paramagnetic and thus incurs a signal drop when its rate increases. Brain activity increases the CBF, but actually this is more governed by the glucose consumption than by the oxygen one. This means that the rate of deoxyhemoglobin/oxyhemoglobin actually decreases, which induces an increase of the MRI signal. In practice, the phenomenon is even more complicated as the CBF increases, blood volume and blood velocity also increase, but the blood oxygenation effect dominates. The signal increase whith current machine is of a few percent at 1.5T and 5-15% for 4T machines.

The BOLD signal is composed of CBF contributions from larger arteries and veins, smaller arterioles and venules, and capillaries. Experimental results indicate that the BOLD signal increases roughly as the square of the magnetic field strength. Furthermore, it can be weighted to the smaller vessels, and hence closer to the active neurons, by using larger magnetic fields. For example, whereas about 70% of the BOLD signal arises from larger vessels in a 1.5 tesla scanner, about 70% arises from smaller vessels in a 4 tesla scanner. This explains the race for larger field scanners: a few 7 tesla commercial scanners have become operational, and experimental 8 and 9 tesla scanners are under development.

5.2 Image Acquisition and Experimental Design

Image acquisition and experimental design are closely coupled. Indeed, the experimental design must be adapted to

[1] As an illustration, the brain receives 15% of the total cardiac output of blood, and yet accounts for 2% of the body weight; in particular, the flow per gram tissue to gray matter is comparable to that in the heart muscle, the most energetic organ in the body [4]. Yet the brain has no reserve store of oxygen, and depends on continuous delivery by CBF.

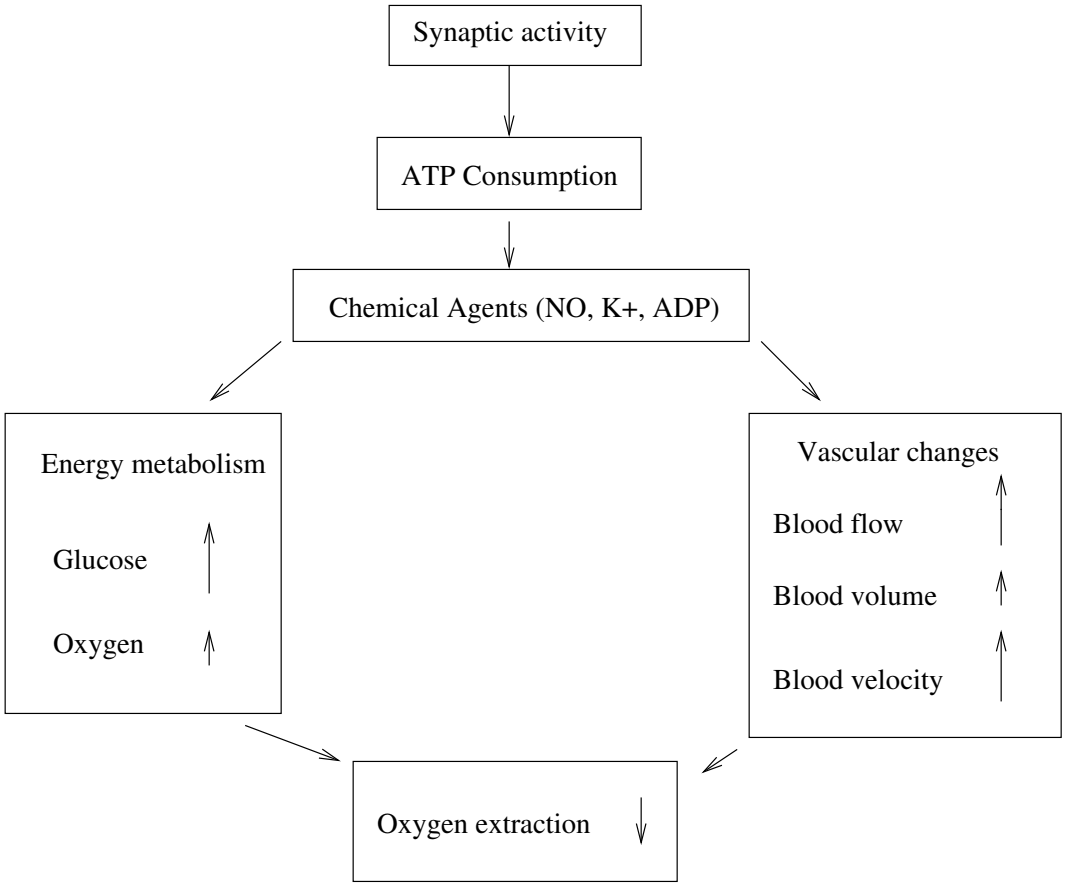

Figure 5.2: Physiological changes accompanying brain activation. Arrows indicate the increase or decrease of the corresponding item and its magnitude. Functional neuroimaging is largely based on the metabolism and flow changes in the lower three blocks: the drop in oxygen extraction is the basis for the BOLD signal changes measured with fMRI, but the MR signal is potentially sensitive to blood flow, volume, and velocity as well. This figure is taken from [4].

5.2.1 Fast MRI sequences

Since functional imaging requires fast acquisition, some techniques have been developed for fast imaging, the most important being echo planar imaging (EPI). In this case, the gradient are oscillated very rapidly, so that sufficient gradient echoes are created to allow measurement of all the phase-encoding steps required for an image. The full data for a low-resolution image are acquired from the signal generated by one RF pulse. EPI requires strong gradients. An 2D image matrix of size 64×64 is acquired in about 30 to 100 ms (instead of a few minutes for a conventional T_2-weighted slice acquisition).

The acquisition of a 3D volume of data is the sequence of multiple slice acquisitions, that can be sequential (ordered in the z direction) or interleaved (pair slices acquired before odd slices)[2].

5.3 Data Preprocessing

We now consider a four-dimensional dataset acquired under a given experimental paradigm. Each volume of data acquired at a given TR is called an image. A set of sequentially acquired images is a run or a session. Many different sessions can be acquired for a given dataset, with repetition of the same experimental paradigm or not. The same experiment can be replicated on many subjects to allow for neurophysiological inference.

5.3.1 Registration

Due to the motion of the subject during the experiment, images have to be registered, so that a given voxel unambiguously represents a brain area for all the images. This involves two steps:

- Motion estimation: it is often assumed that the motion is rigid; this is only approximately true due to the intrinsic artifacts of EPI images that induce non-rigid distortions between images even if the subject motion is rigid. Under this hypothesis, motion estimation boils down to the estimation of six parameters (3 translations, 3 rotations). The most current method consists in finding the rigid transformation that minimizes the grey level difference between consecutive images. This simple method has been shown to introduce artifacts, like spurious task-related motion estimates. More robust methods based on the principle of M-estimator have been designed.

- Motion correction: this step should be performed only when the estimated motion is non-negligible with respect to the voxel size, since a reinterpolation of the data has ill-controlled effects on the data content. The usual method is a trilinear interpolation of the data that takes into account the motion estimates.

[2]Direct 3D acquisition schemes have also been designed. They offer higher Signal to Noise Ratio (SNR), but they do not allow for fast imaging procedures.

Following motion estimation and correction, a step of spatial normalization can be performed: this consists of coregistering the functional images with a MR anatomical image of the same subject or with a template (this is of frequent use for multi-subjects studies), and then to interpolate the functional images into the template. In that case, the displacement field is considered as non-rigid, yielding a heavy computational load. Care should be taken when employing this procedure, because:

- The registration between images or different modalities and/or templates is very difficult. It requires non-rigid deformations (e.g. spatial stretching of the data). The effect on the resulting activation maps may be quite complex.
- This procedure dramatically increases the number of voxels of the dataset, which in turn increases the computation load for the analysis.
- As any sub-sampling procedure, this simply increases the size of the images without adding any information. It is actually simpler to interpolate the final images (activation maps) into the template of interest instead of the raw functional images.

5.3.2 Smoothing

Spatial smoothing has become a standard routine for fMRI data analysis for two kinds of reasons:

- The increase of the SNR: smoothing the data spatially increases the SNR in the sense that it reduces the effect of the spatially uncorrelated noise with respect to a priori more structured signal of interest. This is of course at the expense of spatial precision (the spatial precision of functional images is quite coarse. In particular, the average grey matter width is not much greater than the typical voxel size, so that it is unavoidable that isotropic smoothing mixes tissues of different nature). The debate about spatial smoothing yields a tradeoff between bias (the precision in activation localization) and variance (SNR gain by smoothing). However, it is clear that an optimal smoothing scheme is not the isotropic gaussian filter employed usually, but is brought by adaptative filters.
- The interpretation of the images as gaussian random fields (under the null hypothesis that no activation pattern is present): in the SPM software, activation significance is justified by assuming that the residual of the regression model can be treated as a gaussian random field with a certain smoothness. This is probably not true if one considers the original images, but becomes likely after the smoothing process.

It is important to consider that intrinsic spatial correlation is embedded in raw fMRI datasets. In particular, though many functional brain areas are largely sub-voxel, there is a consensus that reliable activation foci should encompass clustered voxels. Smoothing is then simply a means for canceling spatially high frequency noise in the data. Though this statement is correct, this intrinsic spatial correlation is certainly not isotropic.

5.3.3 Removing global effects

This consists in subtracting to all voxel time courses the mean of each image. This preprocessing is aimed at removing some physiological effects that are assumed to be global over the image. However, this is at the risk of removing activation patterns, if the latter have an influence on the global mean. This is actually the case, and recent studies have enlightened the bias induced by this procedure [7].

5.3.4 Selecting voxels of interest

Signals of interest are expected only in the grey matter. It is thus tempting to ease the analysis by selecting only the anatomically relevant voxels for further analysis. More simply, one often uses a mask that keeps the brain voxels. A simple threshold on the T_2 averaged image of the sequence is often sufficient. More sophisticated methods can be employed, but they are integrated in the general framework of signal analysis.

5.3.5 Detrending

In the temporal part of the dataset also there is the presence of intrinsic correlations. Although some methods use a smoothing in the temporal domain, this is not a systematic usage in fMRI data processing. In fact, the presence of temporal correlations is probably related to the intrinsic object of the measurement, in particular the presence of biological rhythms (respiratory, cardiac) that some authors propose to correct. But there is more consensus on the presence of trends in the signal, which induces high temporal correlation (these effects have typically low frequency) in the dataset. Their cancellation is thus important to enforce the stationarity hypothesis, which is fundamental in the analysis of the data. This is performed by removing the low frequencies of the signal, or by estimating adaptively the trend, or by fitting a wavelet basis.

A practical method is the removal from each voxel-based signal of a fitted low frequency approximation:

$$x_{detrend}(t) = x(t) - (x * g)(t) \tag{5.1}$$

where g is e.g. a gaussian filter wider than the timing of the effects of interest.

5.3.6 Temporal registration or slice timing

Another source of artifacts in the interpretation of the data is the fact that all the slices are not acquired at the same time, but at given fractions of the TR. This effect is problematic when the sequence of events is quick (of the order of the TR). In that case, it may be better to correct for this effect, that is to apply a kind of temporal registration between the slices, so that their acquisition can be considered as simultaneous for further study. This is currently done by preserving the spectrum of the signal obtained at different voxels and shifting their phase. This method has been popularized under the name of *slice timing correction*.

5.4 Generalized Linear Model

Chapter 6

Localizing cortical activity from MEEG

Source localization from external EEG or MEG measurements is an ill-posed inverse problem. Ill-posedness in the sense of Hadamard can have three causes: non-existence, non-uniqueness, and non-continuity with respect to a change in the data. Uniqueness of the source distribution is a well-known problem: there exist "silent sources" of EEG and MEG (see section 4.2.2). However, there are several uniqueness results for the inverse source problem, in the case ideal case of perfect measurements:

- If the source distribution $\mathbf{J}^{\mathrm{p}}$ is modelled as a linear combination of isolated dipoles,

  $$\mathbf{J}^{\mathrm{p}} = \sum_{k=1}^{m} \vec{q}_k \, \delta_{\mathbf{r}_k}(\mathbf{r})$$

  then m, $\vec{q}_k$ and $\mathbf{r}_k$ are uniquely determined by the electric potential V on the whole outer surface (the scalp) [1].

- If $\mathbf{J}^{\mathrm{p}}$ is modelled as a surfacic distribution, and normal to a prescribed surface S: $\mathbf{J}^{\mathrm{p}} = q\mathbf{n}$ then the amplitude of the source distribution, q, is uniquely determined, *up to a constant*, by perfect measurements of the electric potential V on the whole scalp.

Even if the uniqueness of the source distribution giving rise to external measurements can be proved in some cases, in practise, the number of sensors is limited, their response is not perfect, their positions are not perfectly known. The geometrical model is not exact either: the conductivity values are only approximately known, and the sources do not necessarily correspond to the model. Therefore, in practise, regularization is compulsory.

The principle behind all source reconstruction methods is to minimize a norm of the difference between measured and simulated data:

$$C(\mathbf{J}^{\mathrm{p}}) = \left\| \begin{pmatrix} V_{\mathrm{meas}} \\ \mathbf{B}_{\mathrm{meas}} \end{pmatrix} - \begin{pmatrix} V(\mathbf{J}^{\mathrm{p}}) \\ \mathbf{B}(\mathbf{J}^{\mathrm{p}}) \end{pmatrix} \right\| .$$

The relationship between the simulated data $(V, \mathbf{B})$ and the sources $\mathbf{J}^{\mathrm{p}}$ may either be explicit or implicit. The explicit relationship consists in computing the so-called *lead-field matrix*, which relates the sources, discretized in the head volume, to the electromagnetic field at the sensor positions. With a Boundary Element or Finite Element Method, a lead-field matrix computation requires to invert the forward problem matrix. In the case of an implicit relationship, the Poisson equation and Biot-Savart relation are considered as constraints, and incorporated via the technique of Lagrange multipliers (see Appendix A.4, and section **??**).

The sources can be modeled as the superposition of a small number of isolated dipoles, whose number, positions, orientations and amplitudes must be estimated, or as a spatial distribution of dipole parameters over a given region (distributed source) which is discretized over a grid or a mesh.

In the case of isolated dipoles, several models can be chosen to constrain the search. In particular, the spatio-temporal behavior of the dipoles fall into one of three categories:

- *moving dipole*: dipole positions and orientations are both free to vary over time,
- *rotating dipole*: positions are fixed but moment orientations are allowed to vary,
- *fixed dipole*: positions and orientations are both constrained to be fixed.

A difficulty of dipole-based methods is to find the right number of dipoles: an under-estimation will lead to a localization bias, whereas an over-estimation will lead to superfluous dipoles, indistinguishable from the true dipoles, and modify the localizations of the true dipoles.

After presenting the basic, pseudoinverse solution to mean-square minimization in Section 6.1, non-linear dipole fitting methods are presented in Section 6.2. Section 6.3 deals with MUSIC and Beamforming, two scanning methods, which do not rely on an assumption on the number of dipoles. In Section 6.4, we deal with reconstruction methods for distributed sources, where the number of unknowns is far greater than the number of measurements.

6.1 Pseudoinverse solution

The lead-field matrix $\mathbf{G}$ relates the source amplitudes to the (ideal) sensor measurements. In presence of additive measurement noise,

$$\mathbf{M} = \mathbf{G}\mathbf{J} + \mathbf{N} \; . \tag{6.1}$$

Let us make dimensions more explicit: suppose that the number of sensors (both EEG and MEG) equals m, the number of time-points equals n and the source space dimension equals p. Then (6.1) becomes:

$$\begin{pmatrix} M_1(t_1) & \dots & M_1(t_n) \\ \vdots & \ddots & \vdots \\ M_m(t_1) & \dots & M_m(t_n) \end{pmatrix} = \begin{pmatrix} G_{11} & \dots & G_{1p} \\ \vdots & \ddots & \vdots \\ G_{m1} & \dots & G_{mp} \end{pmatrix} \begin{pmatrix} j_1(t_1) & \dots & j_1(t_n) \\ \vdots & \ddots & \vdots \\ j_p(t_1) & \dots & j_p(t_n) \end{pmatrix} + \mathbf{N} \; ,$$

and, denoting as $\mathbf{J}(t_i)$ the column vector $(j_1(t_i) \ldots j_p(t_i))^T$ and $\mathbf{M}(t_i)$ the column vector $(M_1(t_i) \ldots M_p(t_i))^T$,

$$(\mathbf{M}(t_1), \ldots, \mathbf{M}(t_n)) = \mathbf{G}\ (\mathbf{J}(t_1), \ldots, \mathbf{J}(t_n)) + \mathbf{N}$$

The minimum norm solution seeks a source matrix J which minimizes the Frobenius norm

$$\begin{array}{ll} \|\mathbf{M} - \mathbf{G}\,\mathbf{J}\|_F^2 & = Tr\left((\mathbf{M} - \mathbf{G}\,\mathbf{J})^T(\mathbf{M} - \mathbf{G}\,\mathbf{J})\right) \\ & = \sum_i \|\mathbf{M}(t_i) - \mathbf{G}\,\mathbf{J}(t_i)\|^2 \end{array}$$

This problem is equivalent to finding the set $\{J(t_i), i = 1 \ldots n\}$ which, for each i, minimize

$$\|\mathbf{M}(t_i) - \mathbf{G}\,\mathbf{J}(t_i)\|^2 = (\mathbf{M}(t_i) - \mathbf{G}\,\mathbf{J}(t_i))^T\ ((\mathbf{M}(t_i) - \mathbf{G}\,\mathbf{J}(t_i))$$

A simple computation of the gradient with respect to $\mathbf{J}$ shows that a minimizer $\hat{\mathbf{J}}$ of $\|\mathbf{M} - \mathbf{G}\,\mathbf{J}\|^2$ must satisfy

$$\mathbf{G}^T\,\mathbf{G}\hat{\mathbf{J}} = \mathbf{G}^T\mathbf{M}\ . \tag{6.2}$$

If $\mathbf{G}$ has rank p, then $\mathbf{G}^T\,\mathbf{G}$ is invertible and

$$\hat{\mathbf{J}} = \left(\mathbf{G}^T\,\mathbf{G}\right)^{-1}\mathbf{G}^T\mathbf{M}\ .$$

In the case of distributed sources, the source space dimension is generally very large (typically 10^4), while the number of sensors is limited to a few hundred. Hence, $\mathbf{G}$ is rank-deficient, and a minimizer must be selected among the solutions of (6.2). The "Moore-Penrose pseudoinverse" selects the minimizer whose norm is minimum, by imposing $\hat{J}$ to be orthogonal to $Ker\left(\mathbf{G}^T\,\mathbf{G}\right)$. It is denoted

$$\hat{\mathbf{J}} = \left(\mathbf{G}^T\,\mathbf{G}\right)^{\dagger}\mathbf{G}^T\mathbf{M}\ . \tag{6.3}$$

and is computed by Singular Value Decomposition (SVD), as explained in Appendix A.5.

6.2 Dipole fitting

Let us assume a limited number of dipolar sources with fixed position over a time interval. For p dipoles, with position $\mathbf{p}_i$ and moment $\mathbf{q}_i = q_i\mathbf{u}_i$, the relationship between sources and measurements is of the form

$$\mathbf{M}(t) = \sum_{i=1}^{p} g(\mathbf{p}_i, \mathbf{u}_i)\, q_i(t) + \mathbf{N}(t)\ ,$$

or equivalently

$$\mathbf{M}(t) = \mathbf{G}\,\mathbf{Q}(t) + \mathbf{N}(t)\ ,$$

where in this case the lead-field matrix $\mathbf{G}$ is

$$\mathbf{G} = \begin{pmatrix} g_1(\mathbf{p}_1, \mathbf{u}_1) & \dots & g_1(\mathbf{p}_p, \mathbf{u}_p) \\ \vdots & \ddots & \vdots \\ g_m(\mathbf{p}_1, \mathbf{u}_1) & \dots & g_m(\mathbf{p}_p, \mathbf{u}_p) \end{pmatrix}$$

It is possible to separate the direction parameter from the position parameter, by decomposing the lead field over the unit basis: if the coordinates of $\mathbf{u}_i$ in the unit basis are (u_i^x, u_i^x, u_i^x) then $g_j(\mathbf{p}_i, \mathbf{u}_i) = g_j^x(\mathbf{p}_i)\, u_i^x + g_j^y(\mathbf{p}_i)\, u_i^y + g_j^z(\mathbf{p}_i)\, u_i^z$ and the product $\mathbf{G}\, Q$ can be rewritten:

$$\begin{pmatrix} g_1^x(\mathbf{p}_1) & g_1^y(\mathbf{p}_1) & g_1^z(\mathbf{p}_1) & \dots & g_1^x(\mathbf{p}_p) & g_1^y(\mathbf{p}_p) & g_1^z(\mathbf{p}_p) \\ \vdots & \ddots & \vdots & & & & \\ g_m^x(\mathbf{p}_1) & g_m^y(\mathbf{p}_1) & g_m^z(\mathbf{p}_1) & \dots & g_m^x(\mathbf{p}_p) & g_m^y(\mathbf{p}_p) & g_m^z(\mathbf{p}_p) \end{pmatrix} \begin{pmatrix} u_1^x\, q_1 \\ u_1^y\, q_1 \\ u_1^z\, q_1 \\ \vdots \\ u_p^x\, q_p \\ u_p^y\, q_p \\ u_p^z\, q_p \end{pmatrix}$$

The resulting lead field matrix $\mathbf{G}$ thus only depends on the position parameter.
Note: for magnetoencephalography (MEG) in a spherical head model, the measurements do not depend on the radial component of the source, therefore only the two tangential directions need to be computed at each position. The resulting lead field matrix $\mathbf{G}$ has dimension $m \times 2p$ instead of $m \times 3p$ in the general case.

We suppose that

- the number of dipoles p is smaller than the number of sensors m;
- the lead field matrix $\mathbf{G}$ has full rank, thus $\mathbf{G}^T\, \mathbf{G}$ is invertible.

In section 6.1, we have presented the pseudoinverse solution of $\|\mathbf{M} - \mathbf{G}\, \mathbf{Q}\|$:

$$\hat{\mathbf{Q}} = (\mathbf{G}^T\, \mathbf{G})^{-1} \mathbf{G}^T\, \mathbf{M}\ . \tag{6.4}$$

The amplitude term $\mathbf{Q}$ is thus linearly related to the measurements, and easy to compute, once the matrix $\mathbf{G}$ is known. The difficulty is to find the positions $\mathbf{p}_i$ and orientations $\mathbf{u}_i$ of the dipolar sources. Applying $\mathbf{G}$ to both sides of (6.4) shows that

$$\mathbf{G}\, \hat{\mathbf{Q}} = \mathbf{G}\, (\mathbf{G}^T\, \mathbf{G})^{-1} \mathbf{G}^T\, \mathbf{M} \tag{6.5}$$

$$= P_{\mathbf{G}} \mathbf{M} \tag{6.6}$$

is the orthogonal projection of the measurements $\mathbf{M}$ on the range of $\mathbf{G}$, which has dimension $2p$. Hence

$$\|\mathbf{M} - \mathbf{G}\, \hat{\mathbf{Q}}\| = \|\mathbf{M} - P_{\mathbf{G}} \mathbf{M}\| \tag{6.7}$$

6.3 Scanning methods

The methods presented in this section are called scanning methods because they assume that the activated dipole(s) are located at a predefined set of positions. For

example, the considered locations may belong to a regular sampling of the cortex region. The dipole orientations are either assumed to be known or can be left unconstrained. The scanning methods attempt to decide among the possible dipole locations where it is the most appropriate to place the sources so as to best describe some subset of the measurements (usually a small time window containing the events of interest). The two methods presented here rely on different assumptions on the model or on the measured signal and thus cannot be blindly used in all situations[1]. They nonetheless give very stable results when the appropriate conditions are met.

Both methods presented here use a time-window of interest, which needs first to be identified. The signal is also usually prewhitened.

6.3.1 MUltiple SIgnal Classification (MUSIC)

The MUSIC method, proposed in 1992, recovers the positions by scanning potential locations, after having separated a "signal space" from a "noise space" by a Principal Component Analysis (PCA) decomposition [14].

Assuming the sensor space to be of dimensionality m and the time window of size n, an $m \times n$ measurement matrix $\mathbf{M}_k$ is formed for each trial k. As seen above, and assuming, for the time being, that there is no noise, we have $\mathbf{M}_k = \mathbf{G}\mathbf{Q}_k$, where $\mathbf{G}$ and $\mathbf{Q}_k$ are respectively matrices of sizes $m \times r$ and $r \times n$. The number of columns of $\mathbf{G}$, r, is the number of parameters needed to describe the dipoles at all the locations considered to form the matrix $\mathbf{G}$. For example, assuming we have p positions and that only the strengths of the dipoles are to be searched for (the dipole orientations being given), then $r = p$. If orientations as well as orientations are to be recovered, the $r = 3p$. Intermediate situations can also occur. MUSIC is able to treat simultaneously various types of dipoles, but for simplicity we assume here to have only one type of dipole search. Usually, it is assumed that p, and thus r are small with respect to m and n.

MUSIC fundamentally relies on rank assumptions over the matrices $\mathbf{G}$ and $\mathbf{Q}$. More precisely, it is assumed that:

- The $\mathbf{G}$ matrix for p dipoles is full rank (i.e. of rank r) (Gain matrix assumption).
- The correlation matrix $R_{\mathbf{Q}} = E(\mathbf{Q}_k \mathbf{Q}_k^T)$ matrix for p dipoles is full rank (i.e. of rank r) (Asynchronous assumption).
- The noise is considered additive and temporally and spatially zero-mean white noise with variance σ^2 (Noise whiteness). When a good noise model can be established, a prewhitening phase ensures that this is the case. Additionally the signal and noise are assumed to be uncorrelated.

Denoting by $\mathbf{N}_k$ the $m \times n$ noise matrix at trial k, the noisy data $\mathbf{M}_k$ is given by $\mathbf{M}_k = \mathbf{G}\mathbf{Q}_k + \mathbf{N}_k$. The auto-correlation matrix of the measurements $E\left(\mathbf{M}_k \mathbf{M}_k^T\right)$,

[1] This is actually true of every localisation method.

where E denotes the expectation across trials, can be written as:

$$\begin{aligned} E\left(\mathbf{M}_k\mathbf{M}_k^T\right) &= E\left(\left(\mathbf{G}\mathbf{Q}_k+\mathbf{N}_k\right)\left(\mathbf{G}\mathbf{Q}_k+\mathbf{N}_k\right)^T\right) , \\ E\left(\mathbf{M}_k\mathbf{M}_k^T\right) &= E\left(\mathbf{G}\mathbf{Q}_k\mathbf{Q}_k^T\mathbf{G}^T\right)+\mathbf{G}E\left(\mathbf{Q}_k\mathbf{N}_k^T\right)+E\left(\mathbf{N}_k\mathbf{Q}_k^T\right)\mathbf{G}^T+E\left(\mathbf{N}_k\mathbf{N}_k^T\right) , \\ E\left(\mathbf{M}_k\mathbf{M}_k^T\right) &= \mathbf{G}R_{\mathbf{Q}}\mathbf{G}^T+\sigma^2\mathbf{I} , \end{aligned}$$

since $E\left(\mathbf{N}_k\mathbf{Q}_k^T\right) = E\left(\mathbf{Q}_k\mathbf{N}_k^T\right) = 0$ by the assumption that signal and noise are uncorrelated. Since $\mathbf{G}R_{\mathbf{Q}}\mathbf{G}^T$ is exactly of rank r with positive eigenvalue (by the Gain matrix and the asynchronous assumptions), the r highest eigenvalues (and therefore the first r higher singular values of $\mathbf{M}$) correspond to the the signal part of the matrix while the $m-r$ smallest once should (in theory) be identical (equal to σ^2) and correspond to noise.

Using the best rank r approximation of $E\left(\mathbf{M}_k\mathbf{M}_k^T\right)$ thus allows the recovery of the signal space. In practise, MUSIC approximates $E\left(\mathbf{M}_k\mathbf{M}_k^T\right)$ by $\frac{1}{N_k}E\left(\mathbf{M}_k\right)E\left(\mathbf{M}_k\right)^T$, where N_k is the number of trials, which is equivalent to work with the averaged signals. In the following, we denote by $\mathbf{U}$ either the eigenvectors of $\mathbf{F} = E\left(\mathbf{M}_k\mathbf{M}_k^T\right)$ in the "exact" theory or the left singular vectors of $\mathbf{F} = E\left(\mathbf{M}_k\right)$ when $E\left(\mathbf{M}_k\mathbf{M}_k^T\right)$ is approximated by the above formula. In both cases, the column vectors of $\mathbf{U}$ are ordered in such a way that the eigenvalues or the singular values are in decreasing order. The best rank r approximation of $\mathbf{F}$ in terms of the Frobenius norm is simply given by the first r columns of $\mathbf{U}$. Indeed, this corresponds to setting to zero the $m-r$ smallest eigenvalues or singular values of $\mathbf{F}$ (depending on the case).
By writing $\mathbf{U} = [\mathbf{U}_r\mathbf{U}_{m-r}]$, the signal and noise spaces are thus respectively spanned by $\mathbf{U}_r$ and $\mathbf{U}_{m-r}$. By construction, these spaces are orthogonal and the projectors $P_{\mathbf{U}_r} = \mathbf{U}_r\mathbf{U}_r^T$ and $P_{\mathbf{U}_r}^{\perp} = \mathbf{U}_{m-r}\mathbf{U}_{m-r}^T = \mathbf{I} - P_{\mathbf{U}_r}$ can be introduced.

Having identified the signal and noise spaces, the best source locations need to be found. Considering the sub-matrix $\mathbf{G}_i$ corresponding to the columns of $\mathbf{G}$ that are associated with dipole at position x_i, the most appropriate columns are those that best correspond to the subspace $\mathbf{U}_r$. It is equivalent to say that the colums of $\mathbf{G}_i$ should be as orthogonal as possible to $\mathbf{U}_{m-r}$ (it is best to think in terms of angles as otherwise deep sources corresponding to $\mathbf{G}_i$ of small norm would be favored as their contribution to $\mathbf{U}_{m-r}$ will automatically be smaller). Since the matrix $\mathbf{U}_{m-r}^T\frac{\mathbf{G}_i}{\|\mathbf{G}_i\|}$ basically contains all the cosines of all the angles between one vector of the space spanned by $\mathbf{U}_{m-r}$ and one vector of the space spanned by $\mathbf{G}_i$, minimizing the criterion:

$$C(x_i) = \frac{\|\mathbf{U}_{m-r}^T\mathbf{G}_i\|}{\|\mathbf{G}_i\|} ,$$

is what we are looking for as it is equivalent to minimize the sum of the squares of all these cosines. Equivalently, this criterion can be written as:

$$C(x_i) = \frac{\|\mathbf{U}\mathbf{U}_{m-r}^T\mathbf{G}_i\|}{\|\mathbf{G}_i\|} = \frac{\|\mathbf{U}_{m-r}\mathbf{U}_{m-r}^T\mathbf{G}_i\|}{\|\mathbf{G}_i\|} = \frac{\|P_{\mathbf{U}_r}^{\perp}\mathbf{G}_i\|}{\|\mathbf{G}_i\|} ,$$

as $\mathbf{U}$ preserves the norm and as $\mathbf{U}_r\mathbf{U}_{m-r}^T = \mathbf{0}$.

In practise, the image $\frac{1}{C(x_i)}$ is formed and the traditionnal MUSIC method just extracts p maxima from this image as the best locations for the dipoles. This selection scheme is however not very good as the p dipoles extracted may all explain the same part of the signal. Imagine a signal built from the superposition of a superficial source and a deeper one: the above selection scheme will have the tendency to extract sources that all explain the superficial source as it tends to gives the strongest signal, hiding thus the deeper source. For this reason a recursive version of MUSIC called RAP-MUSIC (Recursively APplied MUSIC) has been proposed. In this method, only a single maximum is extracted, and then the signal contribution of this source is substracted from the measurements. The RAP-MUSIC method is then re-applied to this new measurement set.

The advantage of MUSIC over traditional dipole-fitting methods is that it only requires to scan for a single dipole position at a time. Difficulties linked with the MUSIC method are

- its inability to handle spatially distinct but simultaneous sources,
- the distinction between fixed and rotating sources (not described in this text),
- the evaluation of the rank of the gain matrix.

6.3.2 Beamforming methods

Beamforming methods are easier to implement than MUSIC, but rely on an even more restrictive assumption: that sources which are spatially distinct are temporally uncorrelated. The relation between the source amplitudes $J(x_i) = [J^1(x_i)J^2(x_i)J^3(x_i)]$ and the measurements M is given by:

$$\mathbf{M} = \sum_{i=1}^{p} G(x_i) \cdot J(x_i) + \mathbf{N} \ . \tag{6.8}$$

The mean of the source amplitude is denoted $\overline{J(x_i)}$, and the covariance of the source at x_i is defined by

$$C_J(x_i) = E\{[J(x_i) - \overline{J(x_i)}]\,[J(x_i) - \overline{J(x_i)}]^T\}$$

This covariance is a 3×3 matrix whose trace will be used to measure the strength of the source.

Some hypotheses are introduced:

- the noise $\mathbf{N}$ is zero-mean, with covariance C_N.;
- the sources are decorrelated: if $i \neq k$, $E\{[J(x_i) - \overline{J(x_i)}]\,[J(x_k) - \overline{J(x_k)}]^T\}$ is the 3×3 null matrix;
- the noise and the source amplitudes are decorrelated

Under these hypotheses, one can express the mean and covariance of the measurements as:

$$\overline{\mathbf{M}} = E\{\mathbf{M}\} = \sum_{i=1}^{p} G(x_i) \cdot \overline{J(x_i)}$$

$$C_{\mathbf{M}} = E\{[\mathbf{M} - \overline{\mathbf{M}}]\,[\mathbf{M} - \overline{\mathbf{M}}]^T\} = \sum_{i=1}^{p} G(x_i)\, C_J(x_i)\, G(x_i)^T + C_{\mathbf{N}}$$

The concept behind beamforming is, for a given spatial position x_0, to apply a spatial filtering to the measurements, which filters out sources which do not come from a small volume around x_0. Let $W(x_0)$ be a $m \times 3$ matrix representing the spatial filter: the source amplitude in the vicinity of x_0 will be estimated by

$$S(x_0) = (W(x_0))^T \mathbf{M} \; . \tag{6.9}$$

An ideal narrow-band filter should satisfy $(W(x_0))^T G(x) = \mathbf{I}$ if $x = x_0$ and $(W(x_0))^T G(x) = 0$ if not. With such constraints, in the absence of noise, the reconstructed amplitudes $S(x_0)$ would exactly match the source amplitudes $J(x_0)$. However, such an ideal filter response is impossible to achieve with a limited number of measurements m, and a different set of constraints must be sought.

Using (6.8) and (6.9), it is clear that

$$S(x_0) = \sum_{i=1}^{p} (W(x_0))^T G(x_i) \overline{J(x_i)} + (W(x_0))^T \mathbf{N}$$

and taking the covariance of the above expression,

$$\begin{aligned} C_S(x_0) &= \sum_{i=1}^{p} (W(x_0))^T G(x_i) C_J(x_i) (G(x_i))^T W(x_0) + (W(x_0))^T C_N W(x_0) \\ &= C_J(x_0) + \sum_{x_i \neq x_0} (W(x_0))^T G(x_i) C_J(x_i) (G(x_i))^T W(x_0) + (W(x_0))^T C_N W(x_0) \end{aligned}$$

The estimated source strength $Tr(C_S(x_0))$ must match $Tr(C_J(x_0))$. Given the above expression, $Tr(C_S(x_0)) - Tr(C_J(x_0))$ is a positive quantity, and one must therefore seek the $W(x_0)$ which minimizes it.

Given that $Tr(C_J(x_0))$ is independent of $W(x_0)$, the beamforming method seeks $W(x_0)$ which minimizes $Tr(C_S(x_0)) = Tr((W(x_0))^T C_{\mathbf{M}} W(x_0))$, under the constraint that $(W(x_0))^T G(x_0) = \mathbf{I}$.

Using a Lagrange multiplier approach, let L denote a 3×3 matrix of multipliers and introduce the Lagrangian

$$\mathcal{L}(W, L) = Tr(W^T C_{\mathbf{M}} W + (W^T G - \mathbf{I})\, L) \; .$$

At the saddle-point (W, L) of $\mathcal{L}$,

$$W = -\tfrac{1}{2} C_{\mathbf{M}}^{-1} G\, L \; .$$

Substituting this expression in $G^T W = \mathbf{I}$ yields

$$L = -2(G^T C_{\mathbf{M}}^{-1} G)^{-1}$$

therefore

$$W = C_{\mathbf{M}}^{-1} G \left(G^T C_{\mathbf{M}}^{-1} G\right)^{-1}$$

and

$$W^T = \left(G^T C_{\mathbf{M}}^{-1} G\right)^{-1} G^T C_{\mathbf{M}}^{-1}$$

in which we can recognize an expression similar to a "pseudoinverse" of G.

Given the above expression for the spatial filter, computing the estimated source strength $Tr(C_S(x_0))$ leads to considerable simplifications: indeed,

$$\widehat{VarJ(x_0)} = Tr(C_S(x_0)) = Tr\left(\left(G(x_0)^T C_{\mathbf{M}}^{-1} G(x_0)\right)^{-1}\right) \tag{6.10}$$

From this expression, it is clear that the spatial resolution of the reconstruction depends on the spatial resolution of the lead field matrices $G(x_0)$, which in turn depends on the number of sensors and their positions, and on the source positions (superficial sources better resolved than deep sources).

In fact, supposing the measurements to be only due to noise, and $C_{\mathbf{M}} = C_{\mathbf{N}} = \mathbf{I}$: in this case,

$$\widehat{VarJ(x_0)} = Tr\left(\left(G(x_0)^T G(x_0)\right)^{-1}\right);$$

at positions x_0 far away from the sensors, $(G(x_0)^T G(x_0))$ only has small elements, and $Tr\left(\left(G(x_0)^T G(x_0)\right)^{-1}\right)$ can become unduly large, since there is no activity present in this model. To compensate for this, a renormalization is introduced:

$$\widehat{VarJ(x_0)} = \frac{Tr\left(\left(G(x_0)^T C_{\mathbf{M}}^{-1} G(x_0)\right)^{-1}\right)}{Tr\left(\left(G(x_0)^T C_{\mathbf{N}}^{-1} G(x_0)\right)^{-1}\right)} .$$

In conclusion, beamformers offer a rapid exploration of the source space, under strict assumptions of decorrelation between different sources, and between the sources and the noise.

6.4 Estimating distributed activity: imaging approach

In this section, we consider the source to be distributed over a spatial region which describes the cortical mantle, its orientation fixed normal to the cortical sheet, and the source amplitude is to be estimated. This approach was first proposed by Dale and Sereno [6]. In this source model, tens of thousands degrees of freedom are typically needed to represent a source distribution on the surface of the cortex.

When the gain matrix $\mathbf{G}$ can be computed for such source models, it is a rectangular matrix (p columns and m lines with $p \gg m$). We have seen in Section 6.1 a Moore-Penrose pseudoinverse solution to the source estimation problem (6.3). This solution unfortunately has the disadvantage of being unstable with respect to measurement noise and to model errors. This can be seen by considering the condition number of the Moore-Penrose pseudoinverse. Let σ_1 be the largest eigenvalue of $\mathbf{G}^T\mathbf{G}$, and σ_r its smallest non-null eigenvalue: the condition number of $(\mathbf{G}^T\mathbf{G})^\dagger$ is $\frac{\sigma_1}{\sigma_r}$. Inaccuracies due to noise in the measurements can potentially be amplified by this quantity.

The purpose of the regularization which is presented in the next section is to lower this condition number, in order to provide stability of the reconstructed source.

6.4.1 Tikhonov regularization

Instead of minimizing $\|\mathbf{M} - \mathbf{G}\,\mathbf{J}\|^2$, the Tikhonov-regularized problem adds a regularity term to the cost function to be minimized:

$$C_\lambda(\mathbf{J}) = \|\mathbf{M} - \mathbf{G}\,\mathbf{J}\|^2 + \lambda\|\mathbf{J}\|^2 \ .$$

The L^2 norm is the simplest regularization term which may be introduced, but many variants exist. To minimize $C_\lambda(\mathbf{J})$, a necessary condition is that the gradient of C_λ with respect to $\mathbf{J}$ vanishes thus

$$(\mathbf{G}^T\,\mathbf{G} + \lambda\,\mathbf{I})\,\mathbf{J}_\lambda = \mathbf{G}^T\,\mathbf{M} \ .$$

The addition of the regularization term has made the matrix invertible, and the solution to the above equation is therefore $\mathbf{J}_\lambda = (\mathbf{G}^T\,\mathbf{G} + \lambda\mathbf{I})^{-1}\mathbf{G}^T\,\mathbf{M}$. Here the condition number is $\frac{\sigma_1+\lambda}{\lambda}$ which is lower than the condition number of the pseudoinverse as soon as $\lambda > \sigma_r$.

When the number of sources is much greater than the number of sensors, it is computationally efficient to make use of the following trick:

$$\begin{aligned}\mathbf{J}_\lambda &= (\mathbf{G}^T\,\mathbf{G} + \lambda\,\mathbf{I})^{-1}G^T M \\ &= \mathbf{G}^T(\mathbf{G}\,\mathbf{G}^T + \lambda\,\mathbf{I})^{-1}M\end{aligned}$$

6.4.2 Selecting the regularization parameter: the L-curve

In the Tikhonov-type regularization, a parameter λ has been introduced, which must be chosen carefully: if λ is too small, the reconstruction will remain unstable, whereas if λ is too large, the measurements will no longer be properly explained. Selection of the regularization parameter can be performed with the help of the L-curve, which represents in a 2D plane, $\log\|\mathbf{M} - \mathbf{G}\,\mathbf{J}_\lambda\|$ versus $\log\|\mathbf{J}_\lambda\|$, for different values of the parameter λ. The optimal λ is the one for which the curve displays a corner [11].

Appendix A

Useful mathematic formulae and lemma

A.1 Differential operators in $\mathbb{R}^3$

The *nabla* operator is a notation representing $\nabla = \begin{pmatrix} \partial_x \\ \partial_y \\ \partial_z \end{pmatrix}$. The gradient of a scalar field $a(x, y, z)$ is a vector field defined by $\nabla a = \begin{pmatrix} \frac{\partial a}{\partial x} \\ \frac{\partial a}{\partial y} \\ \frac{\partial a}{\partial z} \end{pmatrix}$

Given a vector field $\mathbf{b}$, whose coordinates in the canonical basis of $\mathbb{R}^3$ are the three scalar fields b_x, b_y and b_z: $\mathbf{b} = \begin{pmatrix} b_x \\ b_y \\ b_z \end{pmatrix}$, and The divergence of $\mathbf{b}$ is denoted $\nabla \cdot \mathbf{b}$.

$$\nabla \cdot \mathbf{b} = \frac{\partial b_x}{\partial x} + \frac{\partial b_y}{\partial y} + \frac{\partial b_z}{\partial z}$$

The divergence of the gradient is called the Laplacian:

$$\Delta a = \nabla \cdot \nabla a \ .$$

The curl of vector field $\mathbf{b}$ is denoted $\nabla \times \mathbf{b}$.

$$\nabla \times \nabla \times \mathbf{b} = \nabla(\nabla \cdot \mathbf{b}) - \Delta \mathbf{b} \tag{A.1}$$

where $\Delta \mathbf{b}$ is a vector field whose coordinates are the Laplacian of the coordinates of $\mathbf{b}$.

A.1.1 Conversion from volume to surface integrals

Let Ω be a volume in $\mathbb{R}^3$ and $\partial\Omega$ its boundary. Let $\mathbf{n}$ be an outward-pointing normal field defined on the boundary. Integrating the divergence of a vector field $\vec{f}$ on Ω is

equivalent to summing the flux $\vec{f} \cdot \mathbf{n}$ over the boundary:

$$\int_\Omega \nabla \cdot \vec{f}\, d\mathbf{r} = \int_{\partial\Omega} \vec{f} \cdot \mathbf{n}\, ds \tag{A.2}$$

The above identity is called the Stokes theorem. In particular, if $\vec{f} = \nabla h$, this implies that

$$\int_\Omega \Delta\, d\mathbf{r} = \int_{\partial\Omega} \frac{\partial h}{\partial \mathbf{n}}\, ds\ . \tag{A.3}$$

A similar relationship holds for the curl of a vector field $\vec{f}$, $\nabla \times \vec{f}$:

$$\int_\Omega \nabla \times \vec{f}\, d\mathbf{r} = \int_{\partial\Omega} \mathbf{n} \times \vec{f}\, ds\ . \tag{A.4}$$

In the above surface integral, it is noteworthy that the order is $\mathbf{n} \times \vec{f}$ and *not* $\vec{f} \times \mathbf{n}$.

A.1.2 The Green function for the Laplacian in $\mathbb{R}^3$

The Green function G_L for the Laplacian in $\mathbb{R}^3$ is a solution in $\mathbb{R}^3$ of:

$$\Delta G_L(\mathbf{r}) = \delta_0(\mathbf{r})\ ,$$

where δ_0 denotes the dirac mass positionned at the origin of the space.

Theorem A.1. *The Green function for the Laplacian in $\mathbb{R}^3$ with radial symmetry is:*

$$G_L(\mathbf{r}) = -\frac{1}{4\pi\|\mathbf{r}\|}\ .$$

Proof. To find a solution to this equation, we integrate it over a volume Ω that contains the origin of the space:

$$\int_\Omega \Delta G_L(\mathbf{r})\, d\mathbf{r} = \int_\Omega \delta_0(\mathbf{r})\, d\mathbf{r} = 1\ .$$

Applying the Stokes theorem on the left hand side of this equation leads to:

$$\int_{\partial\Omega} \nabla G_L(\mathbf{r}) \cdot \mathbf{n}\, ds = 1$$

Let us call $r = \|\mathbf{r}\|$ and look for a solution with radial symmetry $G_L(\mathbf{r}) = u(r)$. In this case, the gradient $\nabla G_L(\mathbf{r}) \cdot \mathbf{n}$ is a constant $u_r(R)$ on each sphere of radius R. Applying the above formula to such a spherical domain Ω gives:

$$4\pi R^2 u_r(R) = 1\ .$$

Thus:

$$u_r(r) = \frac{1}{4\pi r^2}\ ,$$

and:

$$G_L(\mathbf{r}) = u(r) = -\frac{1}{4\pi r}\ .$$

□

A.2 The Poincaré and Hölder inequalities

Lemma A.1. ***Hölder inequality:*** *For $u \in L^2(\Omega)$ and $v \in L^2(\Omega)$, we have:*

$$\left(\int_\Omega |uv| \, d\mathbf{r}\right)^2 \leq \int_\Omega u^2 \, d\mathbf{r} \int_\Omega v^2 \, d\mathbf{r}$$

Proof. Since $|uv| \leq \frac{1}{2}\left(u^2 + v^2\right)$, we have:

$$\int_\Omega |uv| \, d\mathbf{r} \leq \frac{1}{2}\left(\int_\Omega u^2 \, d\mathbf{r} + \int_\Omega v^2\right) \, d\mathbf{r}$$

Replacing u by λu in the previous formula, we have:

$$\begin{aligned} \forall \lambda > 0 \int_\Omega |uv| \, d\mathbf{r} &\leq \frac{1}{2}\left(\lambda \int_\Omega u^2 \, d\mathbf{r} + \frac{1}{\lambda}\int_\Omega v^2 \, d\mathbf{r}\right) \\ &\leq \min_{\lambda>0} \frac{1}{2}\left(\lambda \int_\Omega u^2 \, d\mathbf{r} + \frac{1}{\lambda}\int_\Omega v^2 \, d\mathbf{r}\right) \end{aligned}$$

Since the minimum of $\lambda A + \frac{1}{\lambda}B$ for $\lambda > 0$ is obtained for $\lambda = \sqrt{\frac{B}{A}}$, we get:

$$\int_\Omega |uv| \, d\mathbf{r} \leq \sqrt{\int_\Omega u^2 \, d\mathbf{r}} \sqrt{\int_\Omega v^2 \, d\mathbf{r}}$$

□

Remark A.1. *Applying the Hölder inequality for $v = 1$, we obtain:*

$$\left(\int_\Omega |u| \, d\mathbf{r}\right)^2 \leq vol(\Omega) \int_\Omega u^2 \, d\mathbf{r} \, . \tag{A.5}$$

Lemma A.2. ***Poincaré inequality:*** *If Ω is bounded then there is a constant $C(\Omega) > 0$ such that*

$$\forall w \in H_0^1(\Omega) \quad \int_\Omega w^2(\mathbf{r}) \, d\mathbf{r} \leq C(\Omega) \int_\Omega \|\nabla w(\mathbf{r})\|^2 \, d\mathbf{r}$$

Proof. The proof is established here only in the 1D case for $\Omega = [a, b]$. Since $w \in H_0^1(\Omega)$, $w(a) = w(b) = 0$. We have:

$$|w(x)| = |w(x) - w(a)| = \left|\int_a^x w'(\mathbf{r}) \, d\mathbf{r}\right| \leq \int_a^x |w'(\mathbf{r})| \, d\mathbf{r} \leq \int_a^b |w'(\mathbf{r})| \, d\mathbf{r}$$

Integrating the previous equation squared yields:

$$\int_a^b w^2(\mathbf{r}) \, d\mathbf{r} \leq (b-a)\left(\int_a^b |w'(\mathbf{r})| \, d\mathbf{r}\right)^2$$

Using Eq. A.5 for the right hand side of the previous equation, we get:

$$\int_a^b w^2(\mathbf{r}) \, d\mathbf{r} \leq (b-a)^2 \int_a^b w'(\mathbf{r})^2 \, d\mathbf{r}$$

□

A.3 Integral equalities

On a face f defined by the vertices $\mathbf{V}_k$, $k = 1..d+1$, given a base function w^i for some index i, the integral $A_i = \int_f w^i(\mathbf{r})d\mathbf{r}$ is zero (because $w^i = 0$ over f) if the index i does not correspond to one of the vertices defining f. Otherwise, without loss of generality, we assume that i corresponds to the vertex $\mathbf{V}_1$.

Parameterizing the space by the affine basis defined by the vertices $\mathbf{V}_k$, we have $\mathbf{r} = \left(1 - \sum_{j=1}^{d} \lambda_j\right) \mathbf{V}_{d+1} + \sum_{j=1}^{d} \lambda_j \mathbf{V}_j$, where $\lambda = (\lambda_j \ , j = 1 \dots d)$ is the vector of affine parameters. $\mathbf{r}$ is in the domain delimited by f iff all the coefficients in the previous formula are between 0 and 1. Furthermore, $d\mathbf{r} = |\mathbf{V}_1 \dots \mathbf{V}_{d+1}|\, d\lambda$ (the determinant is written with homogenous coordinates for the vectors $\mathbf{V}_k$).

$$
\begin{aligned}
A_i &= \int_f \frac{|\mathbf{r}\ \mathbf{V}_2 \dots \mathbf{V}_{d+1}|}{|\mathbf{V}_1 \dots \mathbf{V}_{d+1}|}\, d\mathbf{r} \\
&= \int_0^1 \int_0^{1-\lambda_1} \dots \int_0^{1-\sum_{i=1}^{d-1}\lambda_i} \left| \left(1 - \sum_{j=1}^{d} \lambda_j\right) \mathbf{V}_{d+1} + \sum_{j=1}^{d} \lambda_j \mathbf{V}_j\ \mathbf{V}_2 \dots \mathbf{V}_{d+1} \right| d\lambda_d \dots d\lambda_1 \\
&= |\mathbf{V}_1 \dots \mathbf{V}_{d+1}| \int_0^1 \int_0^{1-\lambda_1} \dots \int_0^{1-\sum_{i=1}^{d-1}\lambda_i} \lambda_1\, d\lambda_d \dots d\lambda_1 \\
&= \frac{1}{p!} |\mathbf{V}_1 \dots \mathbf{V}_{d+1}| \int_0^1 \lambda_1 \int_0^{1-\lambda_1} \dots \int_0^{1-\sum_{i=1}^{d-p-1}\lambda_i} \left(1 - \sum_{i=1}^{d-p} \lambda_i\right)^p d\lambda_{d-p} \dots d\lambda_1 \\
&= \frac{1}{(d-1)!} |\mathbf{V}_1 \dots \mathbf{V}_{d+1}| \int_0^1 \lambda_1 (1-\lambda_1)^{d-1} d\lambda_1 \\
&= \frac{1}{(d+1)!} |\mathbf{V}_1 \dots \mathbf{V}_{d+1}| \\
&= \frac{1}{d+1} Volume(f)
\end{aligned}
$$

Similarly :

$$
\begin{aligned}
A_i^k &= \int_f \left(\frac{|\mathbf{r}\ \mathbf{V}_2 \dots \mathbf{V}_{d+1}|}{|\mathbf{V}_1 \dots \mathbf{V}_{d+1}|}\right)^k d\mathbf{r} \\
&= |\mathbf{V}_1 \dots \mathbf{V}_{d+1}| \int_0^1 \int_0^{1-\lambda_1} \dots \int_0^{1-\sum_{i=1}^{d-1}\lambda_i} \lambda_1^k\, d\lambda_d \dots d\lambda_1 \\
&= \frac{1}{(d-j)!} |\mathbf{V}_1 \dots \mathbf{V}_{d+1}| \int_0^1 \lambda_1^k \int \dots \int_0^{1-\sum_{i=1}^{j-1}\lambda_i} (1 - \sum_{i=1}^{j} \lambda_j)^{d-j}\, d\lambda_j \dots d\lambda_1 \\
&= \frac{1}{(d-1)!} |\mathbf{V}_1 \dots \mathbf{V}_{d+1}| \int_0^1 \lambda_1^k (1-\lambda_1)^{d-1} d\lambda_1 \\
&= \frac{1}{(d-1)!} |\mathbf{V}_1 \dots \mathbf{V}_{d+1}| \frac{k!(d-1)!}{(d+k)!} \\
&= \frac{k!d!}{(d+k)!} Volume(f)
\end{aligned}
$$

$$
\begin{aligned}
B_i^{kl} &= \int_f \left(\frac{|\mathbf{r}\ \mathbf{V}_2 \dots \mathbf{V}_{d+1}|}{|\mathbf{V}_1 \dots \mathbf{V}_{d+1}|} \right)^k \left(\frac{|\mathbf{V}_1\ \mathbf{r}\ \mathbf{V}_3 \dots \mathbf{V}_{d+1}|}{|\mathbf{V}_1 \dots \mathbf{V}_{d+1}|} \right)^l d\mathbf{r} \\
&= |\mathbf{V}_1 \dots \mathbf{V}_{d+1}| \int_0^1 \int_0^{1-\lambda_1} \dots \int_0^{1-\sum_{i=1}^{d-1}\lambda_i} \lambda_1^k \lambda_2^l \, d\lambda_d \dots d\lambda_1 \\
&= \frac{1}{(d-2)!} |\mathbf{V}_1 \dots \mathbf{V}_{d+1}| \int_0^1 \int_0^{1-\lambda_1} \lambda_1^k \lambda_2^l (1-\lambda_1-\lambda_2)^{d-2} \, d\lambda_2 d\lambda_1 \\
&= \frac{1}{(d+2)!} |\mathbf{V}_1 \dots \mathbf{V}_{d+1}| \text{ for k} = \text{l} = 1
\end{aligned}
$$

A.4 Minimization under contraints: the Lagrange multiplier approach

Suppose one want to solve a constrained minimisation problem such as:

$$\mathbf{x} = \underset{x, f(x)=O}{\operatorname{argmin}} C(x) \,, \tag{A.6}$$

where x can represent a single or vectorial variable, $C(x)$ is the criterion to be minimized and $f(x) = 0$ represents a constraint on the solution x (again this constraint can be either scalar or vectorial). For simplicity, only the scalar version of the problem is developped hereafter. The Lagrange multiplier approach states that problem A.6 can be expressed equivalently as the un-constrained problem:

$$\mathbf{x} = \underset{x,\lambda}{\operatorname{argmin}} C(x) - \lambda f(x); \,, \tag{A.7}$$

The normal equations associated to problem A.7 are:

$$
\begin{cases}
C'(x) - \lambda f'(x) &= 0 \,, \\
f(x) &= 0 \,.
\end{cases}
$$

which clearly shows that the constraint $f(x) = 0$ is taken into account for the solution of the minimization problem. λ is called the Lagrangian parameter. In the vectorial case, as many Lagrangian parameters as constraints must be introduced and the term $\lambda f(x)$ is replaced by a scalar product.

A.5 Singular Value Decomposition

A basic theorem of linear algebra states that any real $M \times N$ matrix $\mathbf{A}$ with $M \geq N$ can be written as the product of an $M \times N$ column orthogonal matrix $\mathbf{U}$, an $N \times N$ diagonal matrix $\mathbf{D}$ with non-negative diagonal elements (known as the *singular values*), and the transpose of an $N \times N$ orthogonal matrix $\mathbf{V}$ [9]. In other words,

$$\mathbf{A} = \mathbf{U}\mathbf{D}\mathbf{V}^T = \sum_{i=1}^{N} d_i \mathbf{U}_i \mathbf{V}_i^T \,, \tag{A.8}$$

where d_i refers to the i-th non-zero element of a diagonal matrix $\mathbf{D}$ and $\mathbf{M}_i$ designates the i-th column of a matrix $\mathbf{M}$ (applied here to the matrices $\mathbf{U}$ and $\mathbf{V}$). The singular values are the square roots of the eigenvalues of the matrix $\mathbf{A}\mathbf{A}^T$ (or $\mathbf{A}^T\mathbf{A}$ since these matrices share the same non-zero eigenvalues) while the columns of $\mathbf{U}$ and $\mathbf{V}$ (the *singular vectors*) correspond to the eigenvectors of $\mathbf{A}\mathbf{A}^T$ and $\mathbf{A}^T\mathbf{A}$ respectively. As defined in Eq.(A.8), the SVD is not unique since:

- It is invariant to arbitrary permutations of the singular values and their corresponding left and right singular vectors. Sorting the singular values (usually by decreasing magnitude order) solves this problem unless there exist equal singular values.
- Simultaneous changes in the signs of the vectors $\mathbf{U}_i$ and $\mathbf{V}_i$ do not have any impact on the leftmost part of Eq.(A.8). In practice, this has no impact on most numerical computations involving the SVD.

In the case where $M < N$, the above theorem can be applied to $\mathbf{A}^T$ yielding basically the same result, with the matrices $\mathbf{D}$ and $\mathbf{U}$ being $M \times M$ and matrix $\mathbf{V}$ being $M \times N$.

If $\mathbf{A}$ is considered as a linear operator from a vector space $\mathbf{E}_N$ of dimension N to a vector space $\mathbf{E}_M$ of dimension M, then SVD can be interpreted as chosing specific orthogonal bases for $\mathbf{E}_M$ (given by $\mathbf{U}$ eventually completed if non square) and $\mathbf{E}_N$ (given by $\mathbf{V}$ eventually completed if non square), such that $\mathbf{A}$ is diagonal (given by $\mathbf{D}$) when expressed in the coordinate frames associated with those bases.

If $\mathbf{A}$ has null singular values (ie $\mathbf{D}$ has null diagonal elements), then this means that $\mathbf{A}$ is singular. Its rank R is exactly equal to the number of non-null singular values. From Eq. (A.8) is then possible to obtain a reduced form of the SVD, in which $\mathbf{U}_R$, $\mathbf{D}_R$ and $\mathbf{V}_R$ are respectively $M \times R$, $R \times R$ and $N \times R$ matrices yielding the general formula:

$$\mathbf{A} = \mathbf{U}_R \mathbf{D}_R \mathbf{V}_R^T = \sum_{i=1}^{R} d_{Ri} \mathbf{U}_{Ri} \mathbf{V}_{Ri}^T \ .$$

The matrices $\mathbf{U}_R$, $\mathbf{D}_R$, $\mathbf{V}_R$ are obtained by taking the columns of matrices $\mathbf{U}$, $\mathbf{D}$, $\mathbf{V}$ corresponding to the non-null elements d_i. Thus, $\mathbf{U}_R$ and $\mathbf{V}_R$ provide respectively orthogonal bases of the image of $\mathbf{A}$ and of the orthogonal to the kernel of $\mathbf{A}$.

Standard libraries such as lapack provide efficient ways of computing the SVD of a matrix $\mathbf{A}$ without having to rely on the matrices $\mathbf{A}\mathbf{A}^T$ and $\mathbf{A}^T\mathbf{A}$ (which is an advantage for both the numerical stability of the result and the computational burden). [9] describes the algorithms for computing such a decomposition. Usually singular values are ordered by decreasing order to remove the permutation ambiguity depicted above.

A.5.1 Moore-Penrose pseudoinverse

If the matrix $\mathbf{A}$ is square and invertible, its inverse is very easily obtained as $\mathbf{A}^{-1} = \mathbf{V}\mathbf{D}^{-1}\mathbf{U}^T$. When some singular values are null, $\mathbf{D}^{-1}$ does not exist, but it is still possible to define $\mathbf{D}^\dagger$ as the diagonal matrix such that:

$$d_i^\dagger = \begin{cases} 1/d_i & d_i \neq 0 \\ 0 & d_i = 0 \end{cases} \tag{A.9}$$

The $N \times M$ matrix $\mathbf{A}^\dagger$ defined as:

$$\mathbf{A}^\dagger = \mathbf{V}\mathbf{D}^\dagger\mathbf{U}^T \ ,$$

is defined whatever is the matrix $\mathbf{A}$ (even for non-square and non-invertible matrices) and is called the Moore-Penrose pseudoinverse of matrix $\mathbf{A}$. From the consideration about the reduced SVD, it can be seen that basically the pseudo inverse behaves as a regular inverse between the sub-spaces defined by $\mathbf{U}_R$ and $\mathbf{V}_R$ and has the same kernel as the original matrix $\mathbf{A}$.

Actually, the Moore-Penrose pseudoinverse can be defined as the unique $N \times M$ matrix $\mathbf{A}^\dagger$ that satisfies the following relations:

$$\mathbf{A}\mathbf{A}^\dagger\mathbf{A} = \mathbf{A} \tag{A.10}$$
$$\mathbf{A}^\dagger\mathbf{A}\mathbf{A}^\dagger = \mathbf{A}^\dagger \tag{A.11}$$
$$\left(\mathbf{A}\mathbf{A}^\dagger\right)^* = \mathbf{A}\mathbf{A}^\dagger \tag{A.12}$$
$$\left(\mathbf{A}^\dagger\mathbf{A}\right)^* = \mathbf{A}^\dagger\mathbf{A} \tag{A.13}$$

where $\mathbf{A}^*$ is the conjugate transpose of $\mathbf{A}$. Equation (A.10) simply states that even if $\mathbf{A}\mathbf{A}^\dagger$ is not the identity, its restriction to the image of $\mathbf{A}$ (defined by its column vectors) is the identity. Equation (A.11) states that $\mathbf{A}^\dagger$ is a weak inverse of $\mathbf{A}$ for the multiplicative semigroup. Equations (A.13) and (A.13) state respectively that $\mathbf{A}\mathbf{A}^\dagger$ and $\mathbf{A}^\dagger\mathbf{A}$ are Hermitian matrices. Another property of interest for us is:

$$\mathbf{A}^\dagger = \lim_{\lambda \to 0} \left(\mathbf{A}^T\mathbf{A} + \lambda\mathbf{I}\right)^{-1} \mathbf{A}^T = \lim_{\lambda \to 0} \mathbf{A}^T \left(\mathbf{A}\mathbf{A}^T + \lambda\mathbf{I}\right)^{-1} \ .$$

Various other properties of the Moore-Penrose pseudoinverse and some proofs of the above claims can be found from
`http://en.wikipedia.org/wiki/Moore-Penrose_pseudoinverse`.

A.5.2 SVD and least-squares problems

Singular Value Decomposition is an important decomposition for least-squares methods because of the orthogonal properties of the matrices $\mathbf{U}$ and $\mathbf{V}$.

Indeed, if one has to solve the problem:

$$\mathbf{x} = \underset{\mathbf{x}, \|\mathbf{x}\|=1}{\operatorname{argmin}} \|\mathbf{A}\mathbf{x}\|^2 = \underset{\mathbf{x}}{\operatorname{argmin}} \frac{\|\mathbf{A}\mathbf{x}\|^2}{\|\mathbf{x}\|^2} \ . \tag{A.14}$$

Lagrange multiplier (see section A.4) are used to solve this problem. The above minimisation is thus equivalent to solving the problem:

$$\mathbf{x} = \underset{\mathbf{x}, \lambda}{\operatorname{argmin}} \|\mathbf{A}\mathbf{x}\|^2 - \lambda \left(\|\mathbf{x}, \|^2 - 1\right) \ .$$

Writing the normal equations of this problem yields:

$$\begin{cases} \left(\mathbf{A}^T\mathbf{A} - \lambda\mathbf{I}\right)\mathbf{x} &= 0 \\ \|\mathbf{x},\|^2 &= 1 \end{cases}$$

Thus the solution $\mathbf{x}$ is an eigenvector of $\mathbf{A}^T\mathbf{A}$. In such a case, the value of the criterion is precisely the corresponding eigenvalue. Since singular values and singular vectors of $\mathbf{A}$ are precisely the eigenvalues and eigenvectors of $\mathbf{A}^T\mathbf{A}$, the above problem is thus minimized for the right singular vector corresponding to the smallest singular value of $\mathbf{A}$. Indeed, introducing the SVD of $\mathbf{A}$ yields[1]:

$$\begin{aligned} \mathbf{x} &= \underset{\mathbf{x},\|\mathbf{x}\|=1}{\operatorname{argmin}} \|\mathbf{A}\mathbf{x}\|^2 \\ &= \underset{\mathbf{x},\|\mathbf{x}\|=1}{\operatorname{argmin}} \|\mathbf{U}\mathbf{D}\mathbf{V}^T\mathbf{x}\|^2 \\ &= \underset{\mathbf{x},\|\mathbf{x}\|=1}{\operatorname{argmin}} \|\mathbf{D}\mathbf{V}^T\mathbf{x}\|^2 \text{ since } \mathbf{U} \text{ is an orthogonal matrix} \\ &= \underset{\mathbf{x}',\|\mathbf{x}'\|=1}{\operatorname{argmin}} \|\mathbf{D}\mathbf{x}'\|^2 \text{ with } \mathbf{x}' = \mathbf{V}^T\mathbf{x} \text{ and since } \mathbf{V}^T \text{ is an orthogonal matrix} \end{aligned}$$

The last two transforms are true since orthogonal transforms (corresponding to orthogonal matrices) preserve the norm, which means that $\|\mathbf{U}\mathbf{z}\| = \|\mathbf{z}\|$ and that $\mathbf{V}^T$ maps the unit sphere to itself. Assuming that the smallest singular value has index l, then the solution to this last problem is $\mathbf{x}' = \mathbf{e}_l$ (the vector with all zero components except at position l where the coordinate is 1). Consequently, the solution $\mathbf{x} = \mathbf{V}\mathbf{x}' = \mathbf{V}\mathbf{e}_l = \mathbf{V}_l$. The solution of th problem is thus given by $\mathbf{V}_l$ the l-th column vector of $\mathbf{V}$, where the index l corresponds to the index of the smallest singular value d_l.

[1]Here, the SVD of an $M \times N$ matrix $\mathbf{A}$ is written in such a way that the matrices $\mathbf{U}$, $\mathbf{V}$ and $\mathbf{D}$ are respectively of sizes $M \times M$, $N \times N$ and $M \times N$. This can always be done by completing $\mathbf{U}$ and $\mathbf{V}$ with some addtional orthogonal columns and $\mathbf{D}$ with zero columns or lines (depending on whether $M < N$ or $M > N$)

Bibliography

[1] A. El Badia and T. Ha-Duong. An inverse source problem in potential analysis. *Inverse Problems*, 16:651–663, 2000.

[2] Sylvain Baillet and Line Garnero. A bayesian approach to introducing anatomo-functional priors in the EEG/MEG inverse problem. *IEEE Transactions on Biomedical Engineering*, 44(5):374–385, May 1997.

[3] L. Baratchart, J. Leblond, F. Mandrea, and E.B. Saff. How can the meromorphic approximation help to solve some 2D inverse problems for the Laplacian? *Inverse Problems*, 15:79–90, 1999.

[4] Richard B. Buxton. *Introduction to Functional Magnetic Resonance Imaging*. Cambridge University Press, 2002.

[5] M. Chafik, A. El Badia, and T. Ha-Duong. On some inverse EEG problems. In M. Tanaka and G. S. Dulikravich, editors, *Inverse Problem in Engineering Mechanics II*, pages 537–544. Elsevier Science Ltd, 2000.

[6] A.M. Dale and M.I. Sereno. Improved localization of cortical activity by combining EEG and MEG with MRI cortical surface reconstruction: A linear approach. *Journal of Cognitive Neuroscience*, 5(2):162–176, 1993.

[7] V. Della-Maggiore, W. Chau, P.R. Peres-Neto, and A.R. McIntosh. An empirical comparison of SPM preprocessing parameters to the analysis of fMRI data. *NeuroImage*, 17(1):19–28, 2002.

[8] O. Faugeras, F. Clément, R. Deriche, R. Keriven, T. Papadopoulo, J. Roberts, T. Viéville, F. Devernay, J. Gomes, G. Hermosillo, P. Kornprobst, and D. Lingrand. The inverse EEG and MEG problems: The adjoint space approach I: The continuous case. Technical Report 3673, INRIA, May 1999.

[9] G.H. Golub and C.F. van Loan. *Matrix Computations*. The John Hopkins University Press, Baltimore, Maryland, second edition, 1989.

[10] Matti Hämäläinen, Riitta Hari, Risto J. IImoniemi, Jukka Knuutila, and Olli V. Lounasmaa. Magnetoencephalography— theory, instrumentation, and applications to noninvasive studies of the working human brain. *Reviews of Modern Physics*, 65(2):413–497, April 1993.

[11] Per Christian Hansen. *Rank-deficient and discrete ill-posed problems: Numerical aspects of linear inversion.* SIAM Monographs on Mathematical Modeling and Computation. SIAM, Philadelphia, 1998.

[12] William James. *The Principles of Psychology.* Harvard: Cambridge, MA, 1890.

[13] Jaakko Malmivuo and Robert Plonsey. *Bioelectromagnetism: Principles and Applications of Bioelectric and Biomagnetic Fields.* Oxford University Press, 1995.

[14] John C. Mosher, Paul S. Lewis, and Richard M. Leahy. Multiple dipole modeling and localization from spatio-temporal MEG data. *IEEE Transactions on Biomedical Engineering*, 39(6):541–553, 1992.

[15] Jean-Claude Nédélec. *Acoustic and Electromagnetic Equations.* Springer Verlag, 2001.

[16] G. Thut, J.R. Ives, F. Kampmann, M. Pastor, and A. Pascual-Leone. A device and protocol for combining TMS and online recordings of EEG/evoked potentials. *J. Neurosci. Methods*, 2005.

Index